Author(s): El-Medani, Samir M.; Makhlouf, Abdelmoneim A.; Moustafa, Hussein; Afifi, Manal A.; Haukka, Matti; Ramadan, Ramadan M.

Title: Spectroscopic, crystal structural, theoretical and biological studies of phenylacetohydrazide Schiff base derivatives and their copper complexes

Year: 2020

Version: Accepted version (Final draft)

Please cite the original version:

El-Medani, S. M., Makhlouf, A. A., Moustafa, H., Afifi, M. A., Haukka, M., & Ramadan, R. M. (2020). Spectroscopic, crystal structural, theoretical and biological studies of phenylacetohydrazide Schiff base derivatives and their copper complexes. Journal of Molecular Structure, 1208, Article 127860. https://doi.org/10.1016/j.molstruc.2020.127860

Journal Pre-proof

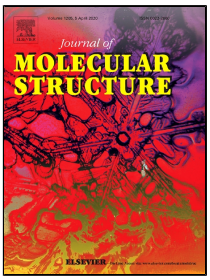

Spectroscopic, crystal structural, theoretical and biological studies of phenylacetohydrazide Schiff base derivatives and their copper complexes

Samir M. El-Medani, Abdelmoneim A. Makhlouf, Hussein Moustafa, Manal A. Afifi, Matti Haukka, Ramadan M. Ramadan

PII:	S0022-2860(20)30184-8
DOI:	https://doi.org/10.1016/j.molstruc.2020.127860
Reference:	MOLSTR 127860
To appear in:	*Journal of Molecular Structure*
Received Date:	06 December 2019
Accepted Date:	04 February 2020

Please cite this article as: Samir M. El-Medani, Abdelmoneim A. Makhlouf, Hussein Moustafa, Manal A. Afifi, Matti Haukka, Ramadan M. Ramadan, Spectroscopic, crystal structural, theoretical and biological studies of phenylacetohydrazide Schiff base derivatives and their copper complexes, *Journal of Molecular Structure* (2020), https://doi.org/10.1016/j.molstruc.2020.127860

Graphical abstract

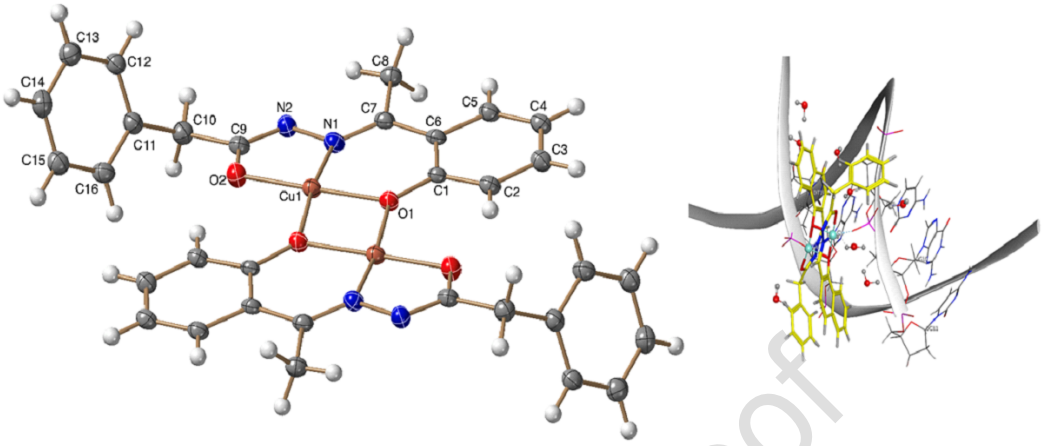

Two phenylacetohydrazide Schiff bases and their Cu(II) complexes were investigated. Optimized structures of the compounds are consistent with the X-ray analysis. The global reactivity descriptors were calculated using DFT. Biological studies including, antimicrobial, antioxidant activities, and fluorescence quenching studies of the complexes were carried out. Molecular docking of the ligands and a copper complex is reported.

Spectroscopic, crystal structural, theoretical and biological studies of phenylacetohydrazide Schiff base derivatives and their copper complexes

Samir M. El-Medani[a,*], Abdelmoneim A. Makhlouf[a], Hussein Moustafa[b], Manal A. Afifi[a], Matti Haukka[c] and Ramadan M. Ramadan[d]

[a] Department of Chemistry, Faculty of Science, Fayoum University, El-Fayoum, Egypt.
[b] Department of Chemistry, Faculty of Science, Cairo University, Giza, Egypt.
[c] Department of Chemistry, University of Jyvaskyla, P.O. Box 35, FI-40014 Jyvaskyla, Finland.
[d] Chemistry Department, Faculty of Science, Ain Shams University, Cairo, Egypt

Abstract:

Two phenylacetohydrazide Schiff base derivatives: N'-(1-(2-hydroxyphenyl)ethylidene)-2-phenylacetohydrazide, **HL1**, and N'-((1-hydroxynaphthalen-2-yl)methylene)-2-phenylacetohydrazide, **HL2**, were synthesized. **HL1** dimerizes in presence of HCl, probably via radical mechanism to give (2,2'-((1E)-hydrazine-1,2-diylidenebis(ethan-1-yl-1-ylidene))diphenol (**DIM**). Thermal reactions of Cu(II) ions with the two Schiff base ligands resulted in formation of the binuclear complexes **$[(CuL1)_2]$** and **$[(CuL2)_2]$**. The stoichiometry and structures of the reported compounds were investigated by several spectroscopic and analytical techniques. The structure of the **HL1** ligand and its complex **$[(CuL1)_2]$** as well as the **DIM** derivative were analyzed by single crystal X-ray analysis. The X-ray analysis revealed the binuclear coordination of the copper complex with the formation of five- and six-membered rings with every ligand. The molecular geometries of the ligands and their copper complexes were investigated using the DFT-B3LYP/GENECP level of theory. The optimized structures of the studied complexes are consistent with the finding of the X-ray analysis. The quantum, non-quantum global reactivity descriptors and the non-linear optical properties were calculated. Biological studies including, antimicrobial and antioxidant activities of the complexes along with fluorescence quenching studies and viscosity measurements are carried out. The molecular docking of the two ligands and **$[(CuL2)_2]$** complex is also reported. The different biological studies as well as molecular docking are correlated to each other and supported the fact that the complexes can bind to DNA via intercalative mode and showed a various DNA binding potency.

Keywords: Copper complexes; X-ray analysis; DFT studies; Antioxidant activity; CT-DNA binding; Molecular docking.

1. Introduction

Schiff base derivatives are important category of organic compounds, which play significant roles in the development of coordination chemistry and can easily form stable complexes with most of transition metals [1-3]. Importance of Schiff bases and their TM complexes, especially those having hydrazide-hydrazone moiety [–(C=O)NHN=CH], are stemmed from their applications as models in biological and bioinorganic chemistry [4,5]. Contribution of these bases as well as their metal complexes are widely used in medicine, drugs, industrial catalysis, chemical analysis, metal corrosion and photochromism [6-8]. Interest in binding of metal complexes to nucleic acids was motivated by the desire to understand the basics of these interaction modes as well as the development of metal complexes to use them as anti-inflammatory and anticancer agents [9]. In particular, hydrazones have found to possess interesting properties such as antimicrobial, anticonvulsant, anti-inflammatory, and antiplatelet, antitubercular and antitumor activities [10-12]. Recently, several series of important hydrazide-hydrazone derivatives were synthesized and found to have promising anticancer activities [13-15]. Also, some transition metal hydrazone complexes such as complexes of Zn(II) and Ni(II) were reported to have anti-inflammatory, antibacterial, anticancer, antihypertensive, and DNA-binding activities [16,17].

Copper and its complexes exhibit considerable biochemical action either as an essential trace metal or as a constituent of various exogenously administered compounds in humans. The copper complexes were also found to be important bioactive species *in vitro* and *in vivo*, which stemmed from the increasing interest in these agents as potential drugs for therapeutic intervention in various diseases [18]. Many copper complexes such as copper-pyridyl-2-carboxamidrazon and copper-4-nitroacetophenone thiosemicarbazone are reported to have potent effect on cancer cells [18]. Thus, the interesting pharmacological properties of these derivatives especially with hydrazone ligands stimulated us to perform the present study. Here, we report the synthesis, spectroscopic, structural and theoretical studies of two hydrazone ligands, **HL1** and **HL2**, derived from phenylacetohydrazide (**Scheme 1**) as well as their Cu(II) complexes. The biological properties of the compounds along with the X-ray analysis of **HL1** ligand and its copper derivative, and the **DIM** derivative are also discussed.

2. Experimental

2.1. Reagents

All chemicals and reagents were of analytical reagent grade and were used without further purification. 2-Phenylacetohydrazide, 2'-hydroxy acetophenone, 2-hydroxy-1-naphthaldehyde and organic solvents were provided from Fluka. Cupric acetate hydrate $Cu(CH_3COO)_2.H_2O$ was provided from Sigma-Aldrich.

2.2. Instrumentation

Infrared measurements were carried out on a Unicam-Mattson 1000 FT-IR spectrometer using KBr discs. Electronic absorption spectra were measured on a Unicam UV2-300 UV-VIS spectrometer. Fluorescence measurements were carried out on a Jenway 6270 Fluorimeter. The excitation source was a Pulsed Xenon Lamp. Nuclear magnetic resonance measurements were performed on a Bruker-BioSpin 300 MHz spectrometer. Samples were dissolved in DMSO-d_6. Magnetic susceptibility values of the copper complexes (Gouy method) were performed using a Sherwood Scientific magnetic susceptibility balance. Elemental analyses were carried out on a Perkin-Elmer 2400 CHN elemental analyzer. Mass spectra of the solid complexes (70 eV, EI) were carried out on a Finnigan MAT SSQ 7000 spectrometer. Bruker BioSpin GmbH was used to record the electron spin resonance spectra at 25 ^oC in the X-band frequency 9.714 GHz, and on a microcrystalline powder with microwave power around 2.012 mW. Thermogravimetric analysis were carried out under nitrogen atmosphere with a heating rate of 10 ^oC/min using a Schimadzu DT-50 thermal analyzer. Conductivity measurements were performed in DMSO ($1x10^{-3}$ M) at 25 ^oC, by using Jenway 4010 conductivity meter.

2.3. Synthesis of compounds

2.3.1. Preparation of N-(1-(2-hydroxyphenyl)ethylidene)-2-phenylacetohydrazide, ***HL1****.*

A mixture of 2-phenylacetohydrazide (0.01 mol, 1.5 g) and 2'-hydroxy acetophenone (0.01mol, 1.2 ml) was refluxed in absolute ethanol for 3 h at which a yellow product was separated. The residue was filtered off, washed with cold ethanol for several times and then recrystallized from hot ethanol to give a crystalline yellow product (yield = 80 %). Chemical formula: $C_{16}H_{18}N_2O_3$;

mol. wt., 286.33; mass spectrometry m/z, 269 $[P\text{-}H_2O]^+$; CHN, found (calc.): %C, 67.04 (67.12), %H, 6.38 (6.34), %N, 9.66 (9.78). IR, cm^{-1}. υ(OH), 3493 (s); υ(NH), 3328 (m), 3223 (m); υ(C=O), 1666 (s); υ(C=N), 1606 (s); ν(C-O), 1250 (m), υ(N-N), 1074. ^{1}H NMR, ppm: 12.86 (bs, 1H, OH), 12.62 (bs, 1H, NH), 6.94-7.78 (m, 9H, aromatic H), 3.64 (s, 2H, CH_2), 2.36 (s, 3H, CH_3).

2.3.2. Preparation of (2,2'-((1E)-hydrazine-1,2-diylidenebis(ethan-1-yl-1-ylidene))diphenol, ***DIM***

A mixture of 2'-hydroxy acetophenone (0.01mol, 1.2 ml), 2-phenylacetohydrazide (0.01 mol, 1.5 g) and two drops of conc. HCl was refluxed in methanol for 4 h. The isolated yellow crude was filtered and washed several times with methanol. Yellow crystalline product was obtained after recrystallization from hot ethanol with a yield of 65 %. Chemical formula: $C_{16}H_{16}N_2O_2$; mol. wt., 268.32; mass spectrometry m/z, 269 $[P]^+$; CHN, found (calc.): %C, 71.55 (71.62), %H, 6.23 (6.01), %N, 10.31 (10.44). IR, cm^{-1}: υ(C=N), 1604, 1558; υ(C-O), 1240; υ(N-N), 1034. ^{1}H NMR, ppm: 12.93 (bs, 2H, 2OH), 7.80-6.98 (m, 8H, aromatic H), 2.51 (s, 6H, $2CH_3$).

2.3.3. Preparation of N'-((1-hydroxynaphthalen-2-yl)methylene)-2-phenylacetohydrazide*,* ***HL2****.*

Similar procedure as that used for the preparation of **HL1** was performed with the use of a mixture of 2-phenylacetohydrazide (0.01 mol, 1.5 g) and 1-hydroxy-2-naphthaldehyde (0.01mol, 1.72 ml). Yellow crystalline product was separated after recrystallization from ethyl acetate (yield = 75 %). Chemical formula: $C_{19}H_{16}N_2O_2$; mol. wt., 304.35; mass spectrometry m/z, 305 $[P]^+$; CHN, found (calc.): %C, 74.77 (74.98), %H, 5.42 (5.30), %N, 9.12 (9.21). IR, cm^{-1}. υ(OH), 3435 (b); υ(NH), 3311(m), 3199 (s); υ(C=O), 1666 (s); υ(C=N), 1623 (m), 1597 (m); ν(C-O), 1270 (m); υ(N-N), 1077. ^{1}H NMR, ppm: 12.51 (bs, 1H, OH-keto), 11.58 (bs, 1H, OH-enol), 11.35 (s, 1H, OH-enol), 10.91 (bs, 1H, NH), 9.22 (s, 1H, CH=N-keto), 8.91 (s, 1H, CH=N-enol), 7.18–8.25 (m, 10H, aromatic), 4.00 (s, 2H, CH_2-keto), 3.62 (s, 2H,CH_2-enol).

2.3.4. Synthesis of ***[(CuL1)$_2$]*** *and* ***[(CuL2)$_2$]*** *complexes*

The two copper complexes, **[(CuL1)$_2$]** and **[(CuL2)$_2$]**, were synthesized by adding an ethanolic solution of $Cu(CH_3COO)_2.H_2O$ (4 mmol; 0.80 g) drop wise to 4 mmol of an ethanolic solution of the ligand. The reaction mixture was refluxed for 3 hours. The solution was left to stand at room temperature for few hours. The green solid complexes formed were isolated by filtration, washed several times with hot ethanol followed by ether. **[(CuL1)$_2$]** was recrystallized from ethanol and **[(CuL2)$_2$]** from DMF (yields of 85 % and 60 %, respectively).

[(CuL1)$_2$]: Chemical formula: $Cu_2C_{32}H_{28}N_4O_4$; mol. wt., 659.70; mass spectrometry m/z, 660 $[P]^+$; CHN, found (calc.): %C, 58.11 (58.26), %H, 4.35 (4.28), %N, 8.23 (8.49). IR, cm^{-1}. υ(C=O), 1596 (m), 1545 (s); υ(C=N), 1515 (s), 1494 (m); ν(C-O), 1230 (m); ν(Cu-O), 590-500 (w); ν(Cu-N), 456-427 (w).

[(CuL2)$_2$]: Chemical formula: $Cu_2C_{38}H_{28}N_4O_4$; mol. wt., 731.76; mass spectrometry m/z, 732 $[P]^+$; CHN, found (calc.): %C, 62.33 (62.37), %H, 3.94 (3.86), %N, 7.49 (7.66). IR, cm^{-1}. υ(C=O), 1617 (s), 1605 (s); υ(C=N), 1538 (m), 1518 (m); ν(C-O), 1191 (m); ν(Cu-O), 594-500 (w); ν(Cu-N), 452-437 (w).

2.4. X-ray structure analysis

Single crystals of **HL1**, **DIM** and **[(CuL1)$_2$]** complex suitable for X-ray diffraction were acquired by slow evaporation of dilute ethanolic solutions at room temperature. The crystals were immersed in cryo-oil, mounted in a MiTeGen loop. The X-ray diffraction data was collected on a Bruker KAPPA APEX II CCD diffractometer using Mo Kα radiation (λ= 0.71073 Å). Cell refinements and data reductions were performed using the Denzo/Scalepack program package [18]. The structures were solved by the charge flipping method using the SHELXT program. A multi-scan absorption correction based on equivalent reflections (SADABS-2012/1) [19] was applied to the data. Structural refinement was carried out using SHELXL-2014 [20] with the UCSF Chimera [21] and SHELXLE-2014 graphical user interfaces. Data collection was carried out at 120(2) K. Temperature was controlled by an Oxford Cryostream cooling system (Oxford Cryostat). Cell refinement and data reduction were performed using the program SAINT [22]. The data were scaled and absorption correction performed using SADABS [23]. The structures were solved by direct methods using SHELXS-97 and refined by full-matrix least-squares methods based on F2 using SHELXL-97 [20] and the graphics interface program X-Seed [20]. All non-hydrogen atoms were refined anisotropically. All hydrogen atoms were positioned geometrically and constrained to ride on their parent atoms with CH= 0.95-0.99 Å and Uiso=1.2-1.5, Ueq (parent atom). The crystallographic data of the ligand **HL1** and its copper complex, **[(CuL1)$_2$],** as well as for the **DIM** are presented in **Table 1**.

2.5. Computational studies

All computations were carried out using Gaussian 09W software package. B3LYP/GENECP method using double zeta plus polarization basis set 6-31G (d,p) for C, H, N,

and O atoms and LANL2DZ basis set for Cu-atoms was used to calculate the geometries of the ligands and the two copper complexes. Electronegativity, χ, chemical hardness, η, electrophilicity, global softness, ionization potential and electron affinity were calculated by using the HOMO and LUMO energy values. The surface area grid (SAG), molar volume (MV), hydration energy (HE), polarizability (Pol) and molar refractivity (MR) were performed using Hyper Chem 8.0.7. The natural bond orbital (NBO) has been performed to measure the qualitative intermolecular delocalization in complexes. The total static dipole moment, (μ), the mean polarizability, <α>, the anisotropy of the polarizability, Δα, and the mean first-order hyperpolarizability, <β >, using the x, y, z components were as reported in literature [23].

2.6. Biological activity studies

2.6.1. Antimicrobial Activity

The ligands and their copper complexes were tested *in vitro* for their antibacterial and antifungal activities with the use of agar well diffusion method. Experimental details of the investigations are as described previously [2]. The antibacterial activity was screened against two bacterial species, one gram-positive (*Staphylococcus. Aureus)* and one gram-negative (*Escherichia coli*). The antifungal activity was screened against two fungal strains (*Aspergillusflavus* and *Candidaalbicans*). Ampicillin and Amphotericin B used as standards for the antibacterial and antifungal activity, respectively. The measurements were performed in triplicate measurements for each compound, and their average values are reported.

2.6.2. Antioxidant assay (DPPH free radical scavenging activity)

In vitro antioxidant activities of the two copper complexes were evaluated using scavenging the stable DPPH radical modified method [25]. DPPH˙ radical scavenging test relies on the absorbance change of the radical when deactivated by antioxidants. It is easily observed with naked eye as color changes from purple to yellow. Stock solutions of the investigated complexes were dissolved in methanol-DMSO (5:1) and then diluted to final concentration of 200, 150, 100, 50 and 10 μM. Methanolic DPPH (2,2-diphenyl-1-picrylhydrazyl) solution (1mL, 0.5 mmol) was added to 5.0 mL of the complex solution as well as to the standard compound (ascorbic acid). Detailed procedure for the DPPH free radical scavenging activity studies is previously given [2].

2.6.3. DNA-binding Studies

The Calf thymus (CT-DNA) binding experiments of the two copper complexes were conducted at ambient temperature. All the experiments involving with the interaction of the complexes with CT-DNA were carried out in a doubly distilled water buffer containing 5 mM Tris-(hydroxylmethyl)aminomethane, stored at 4 ºC and used within 4 days. The UV-Vis absorption ratio of CT-DNA solution A_{260}/A_{280} gives a ratio of 1.8-1.9, indicating that the DNA was sufficiently free from protein. The concentration of CT-DNA per nucleotide was calculated from its absorption intensity using the extinction coefficient of 6600 M^{-1} cm^{-1} at 260 nm [26]. Stock solutions of the complexes were prepared in DMSO and diluted with the corresponding buffer to the required concentrations. The extent of DMSO in the final concentration did not exceed 0.1 %. At this concentration, DMSO has no effect on DNA conformation.

2.6.4. Fluorescence quenching measurements

DNA competitive binding studies with ethidium bromide solution (EB) were carried out at different concentrations (1.0 - 8.0×10^{-5} M) and the concentrations of EB and CT-DNA was kept constant (1.0×10^{-5} M for each). Before measurements, the resulting solutions were shaken up and incubated for 30 min. Details for the procedure and measurements are described previously [2,27].

2.6.5. Viscosity measurements

Viscosity experiments were performed by using Ostwald viscometer immersed in a water bath maintained at a constant temperature (30.0 ± 0.1 ^{o}C). CT-DNA samples of approximately 0.5 mM were prepared by sonication in order to minimize complexities arising from CT-DNA flexibility. Flow time was measured with an automated timer three times for each sample and an average flow time was calculated. Data were presented as $(\eta/\eta_o)^{1/3}$ versus the ratio [complex]/[DNA], where η and η_o are the viscosities of CT-DNA solution in presence and absence of the complex, respectively. Viscosity values were calculated after correcting the flow time of buffer alone (t_o), $\eta= (t-t_o)/t_o$.

2.7. Molecular docking of compounds

The docking studies were performed on Dell Precision™ T3600 Workstation [Intel Xeon E5-1660 3.3GHz, 16GB 1600MHz DDR3, ECC RDIMM 1TB (7200RPM), 1GB NVIDIA Quadro 2000, Windows 7 Professional (64 Bit)]. Molecular Operating Environment (MOE) package version 2016.08 was used to perform docking studies. X-ray crystal structure of a B-DNA dodecamer

d(CGCGAATTCGCG)$_2$ running 3'-5' direction (PDB ID: 1BNA) at 1.9 Å resolution. The DNA structure was opened in MOE, hydrogen atoms were inserted and subsequently energy optimization was carried out. The resulting model afforded to systematic conformational research with RMS gradient of 0.01 kcal/mol^{-1} using default parameters in the Site Finder tool implicated in MOE software.

3. Results and Discussion

The two Schiff base ligands (**HL1** and **HL2)** and their copper complexes **[(CuL1)$_2$]** and **[(CuL2)$_2$]** as well as the **DIM** derivative were synthesized and characterized using different spectroscopic techniques (IR, ^{1}H NMR, mass), elemental analyses, magnetic measurements, molar conductance, and thermal analysis. Elemental analyses and mass spectra data of the reported compounds were in accordance with the proposed molecular formulas. The molar conductivities of 1x10^{-3} M solutions of the two copper complexes at 25 ^{o}C were found to be in the range 11-15 Ω^{-1}mol^{-1}cm^2 indicating the non-electrolyte behavior of these derivatives and the ligand anions are directly bonded to the Cu(II) centers neutralizing their charges. The magnetic susceptibility measurements for the two copper complexes, **[(CuL1)$_2$]** and **[(CuL2)$_2$]**, at 298 K gave effective magnetic moment (μ_{eff}) values = 2.03 and 2.44 BM, respectively. These values are smaller than the spin-only value of two unpaired electrons (2.83 BM) for each complex. The observed lower magnetic moments values could be due to antiferromagnetic coupling between the two cooper centers in the complex. In addition, the structure of **HL1** and its copper complex, **[(CuL1)$_2$]** as well as **DIM** derivative were investigated by single crystal X-ray analysis. It is worth to mention that when we tried to prepare **HL1** as described in literature [28] by refluxing a mixture of 2'-hydroxyacetophenone and 2-phenylacetohydrazide in methanol with the addition of two drops of conc. HCl, **HL1** ligand was not produced. Instead, a dimer (2,2'-((1*E*)-hydrazine-1,2-diylidenebis(ethan-1-yl-1-ylidene))diphenol, **DIM**, with the formula $C_{16}H_{16}N_2O_2$ was obtained. However, **HL1** was prepared by refluxing a mixture of 2'-hydroxyacetophenone and 2-phenylacetohydrazide in absolute ethanol without the addition of acid.

3.1. Spectroscopic studies

The IR spectra (KBr pellets) of the reported compounds were recorded in the region 4000-400 cm^{-1}. The most prominent IR and ^{1}H NMR spectral data for **HL1**, **DIM** and **HL2** are given in the experimental section. The IR spectrum of the **HL1** displayed stretching frequency bands at 3493, 3228, 3223, 1666, (1606 amide I, 1549 amide II) 1250 and 1074 cm^{-1}, which are assigned

to υ(OH), υ(NH), υ(C═O), υ(C═N), υ(C-O) and υ(N-N), respectively [2,29]. Also, the IR spectrum of **HL2** ligand exhibited a pattern of stretching vibration bands similar to that of **HL1**. Therefore, the IR spectra of the ligands in the solid state indicated that they existed in a keto form structure (**Scheme 1**).

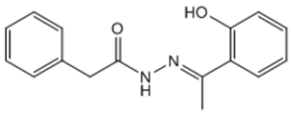

HL1 (solid and solution)

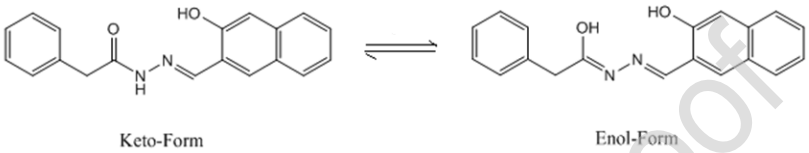

Keto-Form Enol-Form

HL2 (solution)

Scheme 1. The proposed structure of **HL1** and **HL2**.

The ^{1}H NMR studies of the two ligand **HL1** and **HL2** in DMSO showed that they behaved differently in solution. The ^{1}H NMR spectrum of **HL1** displayed only two broad singlets at 12.86 and 12.62 ppm due to the OH and NH protons [30]. Although the signals of the OH and NH moieties were broad, the proton exchange was slow at the NMR time scale and the enol form was not detected. These signals disappeared on addition of D_2O to the DMSO solution. Thus, the appearance of only two signals confirmed that the **HL1** ligand existed mainly in solution as a keto form (**Scheme 1**). We could not rule out the chance of enol formation in solution, because the **HL1** ligand coordinated to copper ion with an enol form (*vide infra*). In addition, the ^{1}H NMR spectrum of **HL1** exhibited multiplets due to the aromatic protons as well as signals due to the methyl and methylene moieties. On the other hand, the ^{1}H NMR spectrum of **HL2** displayed a set of four broad singlets at 12.51, 11.85, 11.35 and 10.91 ppm due to OH and NH protons (**Fig. 1**). These signals were disappeared on addition of D_2O (**Fig. 1 B**). The line broadening of the four signals with the same rate confirmed that the OH and NH proton are exchangeable, i.e, the compound is fluxional at the NMR time scale. Thus, **HL2** existed in solution in two tautomeric (keto/enol) forms, **Scheme 1** [31]. The fact that **HL2** is existing in two forms is also confirmed from the appearance of two azomethine (CH=N) and two CH_2 signals. Furthermore, the ^{1}H NMR spectrum of **HL2** showed signals corresponded to aromatic protons.

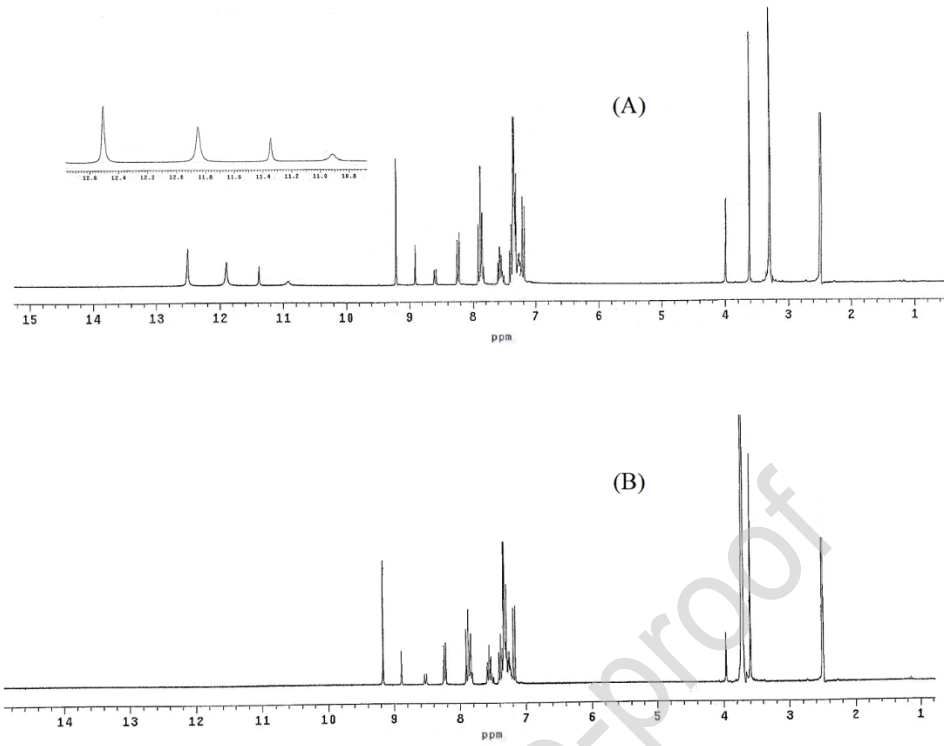

Fig. 1. The ^{1}H NMR spectrum of **HL2** ligand.

The IR spectrum of the **DIM** molecule exhibited stretching frequency bands due to the C=N, C-O and N-N functional groups. Interestingly, the IR spectrum did not illustrate any bands due to the OH groups. Many previous reports indicated the absence of the phenolic groups of the Schiff bases in their IR spectra [32]. This was due to the existence of hydrogen bonding. The ^{1}H NMR spectrum of the **DIM** showed a slightly broad singlet at 12.93 ppm corresponding to the OH protons. This signal was disappeared when the D_2O was added to the DMSO solution. In addition, the spectrum of the compound displayed multiplets (7.80-6.98 ppm) for the aromatic hydrogens and a broad singlet at 2.51 for the methyl groups.

A speculated mechanism for the formation of **DIM** molecule from **HL1** is illustrated in **Scheme 2**. This could be proceeded via acid catalyzed homolyptic fission of the N-NH bond to form the two intermediate radicals **(I)** and **(II)**. Dimerization of two moieties of intermediate **(I)** will led to the formation of **DIM** molecule. On the other hand, interaction of intermediate **(II)** with HCl would give the soluble amine chloride **(III)**.

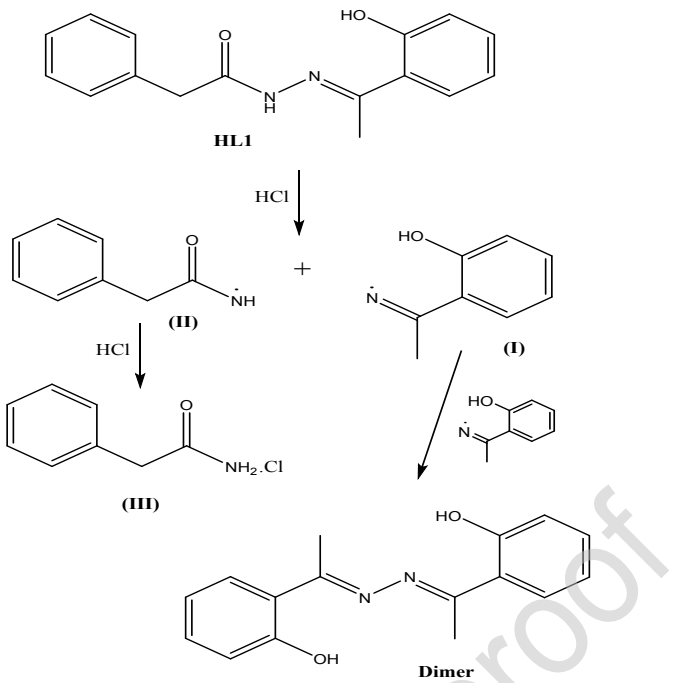

Scheme 2. Proposed mechanism for the formation of the dimer derivative.

Interaction of Cu(II) ions with either **HL1** or **HL2** resulted in the formation of binuclear complexes. The stretching vibration bands of the OH and NH moieties of the free **HL1** and **HL2** were disappeared from the IR spectra of the complexes, which indicated that the ligands coordinated to copper from their O and N donor atoms [2]. The shifts in the bands of the other functional groups, such as C=N and C-O, towards low frequencies also confirmed such conclusion. It is obvious that the two ligands were in their enol form when they coordinated to the copper ion. Furthermore, the IR spectra of the two complexes displayed new non-ligand bands for symmetrical and asymmetrical stretching frequencies of the Cu-O and Cu-N parts due to complex formation [33].

Electron spin resonance (ESR) is a useful tool for investigating the structure and dynamics of molecular systems containing paramagnetic center. The ESR spectra of the reported microcrystalline powder copper complexes **[(CuL1)$_2$]** and **[(CuL2)$_2$]** (**Fig. 2**) were recorded at room temperature on the Klystron X-band at frequency 9.714 GHz, and with microwave power around 2.012 mW and the g factors were measured relative to the standard indicator DPPH (g = 2.0037). The ESR signals in parallel and perpendicular regions appeared as one signal or partially resolved signal due to either distortion in geometry or electron-spin-nuclear-spin coupling. The spectra of the two complexes, **[(CuL1)$_2$]** and **[(CuL2)$_2$]**, displayed the same g// value (g// = 2.15),

while the g⊥ values were equal to 2.09 and 2.08 for the two complexes, respectively. According to Kivelson and Neiman, the g// value in the Cu(II) complex can be used as a measure of covalent characteristics of the metal-ligand bond [34]. For the ionic case the g// value is generally ≥ 2.3, while for covalent state it is < 2.3 [34]. Since the value of g// of the two copper complexes is smaller than 2.3, the Cu(II)-ligand bonds have a considerable covalent properties. The fact that g// > g⊥ > 2.003 for the two complexes indicated that the unpaired electron is mainly localized in the d_{x2-y2} orbital of the copper(II) ion [35]. The geometric factor G is a measure of exchange interaction between the copper centers in the solid compounds. The G factor can be calculated using the expression [36]:

$$G = (g// - 2.0023) / (g\perp - 2.0023)$$

If the value of G is larger than 4, the exchange interaction between copper(II) centers considers negligible. On the other hand, if G is smaller than 4, a significant exchange interaction can be specified in the complex. The calculated G factors for the present complexes, **[(CuL1)$_2$]** and **[(CuL2)$_2$]**, are 1.69 and 1.90 indicating a significant exchange interaction between the copper ions.

3.2. X-ray crystallographic studies

The crystal structure of the three derivatives **HL1**, **DIM** and **[(CuL1)$_2$]** were determined by X-ray analysis. Accurate lattice parameters were determined from least squares refinements of well-centered reflections in the ranges 2.579° ≤ θ ≤ 36.314°, 4.313° ≤ θ ≤ 77.010° and 2.931° ≤ θ ≤ 77.380°, respectively. During data collection, three standard collections were periodically observed without significant intensity variations. The collected reflections were found to be 45765, 15508 and 14086 while the independent reflections were 7089, 2817 and 2761, respectively with I >2:00σ(I). These observed reflections were used for structure determination and refinements. The ranges of h, k and l for the three compounds are -11<=h<=11, -13<=k<=13, -42<=l<=42, -7<=h<=6, -16<=k<=16, -20<=l<=19 and -18 ≤ h ≤ 19; -5 ≤ k ≤ 5, -23 ≤ l ≤ 19, respectively. The crystallographic data for the three derivatives are summarized in **Table 1**, while selected bond lengths and bond angles are given in **Table 2**. The crystallographic analysis showed that both **HL1** and **[(CuL1)$_2$]** complex crystallized in monoclinic $P2_1/n$ space group with a Z value of 4 and 2, respectively, while the **DIM** crystallized in Orthorhombic $P2_12_12_1$ space group with a Z value of 4.

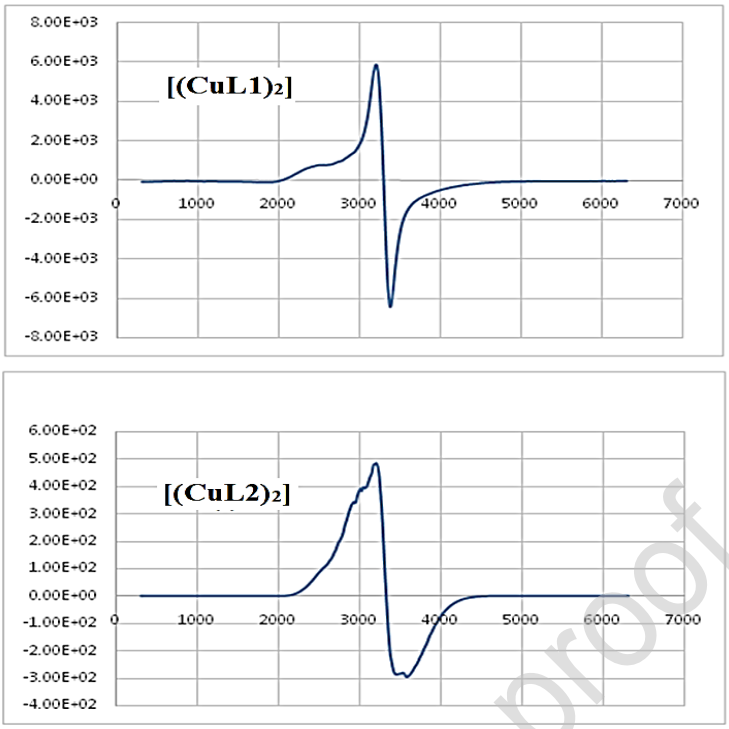

Fig. 2. The ESR spectra of the copper complexes

The ORTEP representation of **HL1** ligand (**Fig. 3**) showed that it crystallized with a water molecule. The structure of the ligand is not planer and the molecule as a whole is unsymmetrical (C_s system). The phenolic, azomethine, N-N and C=O moieties are almost in the same plane, while the benzyl part of the molecule is perpendicular to the plane; the dihedral angle C(1)-C(6)-C(7)-N(1) is 178.9°, while that of N(2)-C(9)-C(10)-C(11) is 88.69°. Also, the angles C(7)-N(1)-N(2), C(9)-N(2)-N(1), O(1)-C(1)-C(6), C(1)-C(6)-C(7), N(1)-C(7)-C(6), O(2)-C(9)-N(2), and O(2)-C(9)-C(10) have values around 120°. These values are corresponding to sp^2 hybridization and confirming that this part of the molecule is nearly in the same plane. The bond lengths of C(7)-N(1) in the azomethine and N(1)-N(2) groups are 1.2944 Å and 1.3723 Å, respectively, which are in the normal range of double and single bond characters [37,38]. Furthermore, the bond lengths of C(9)-O(2) and C(1)-O(1) are found to be 1.2296 Å and 1.3629 Å confirming a double and a single bond for the two groups, respectively. All the other bond lengths and bond angles lie in the normal ranges observed for similar compounds. The content of the unit cell of **HL1** crystal showed that the molecules are arranged with a net of hydrogen bonds involving the crystalized water molecule, **Fig. 4**. It showed the presence of hydrogen bonding between H(1) and N(1) to form an O(1)…H(1)…N(1) moiety as well as a hydrogen bonding between the ketonic oxygen, O(2), and

one of the hydrogen of the water molecule. **Table 3** illustrates the van der Waal displacement between H, the donor (D) and the acceptor (A) as well as the DHA angle.

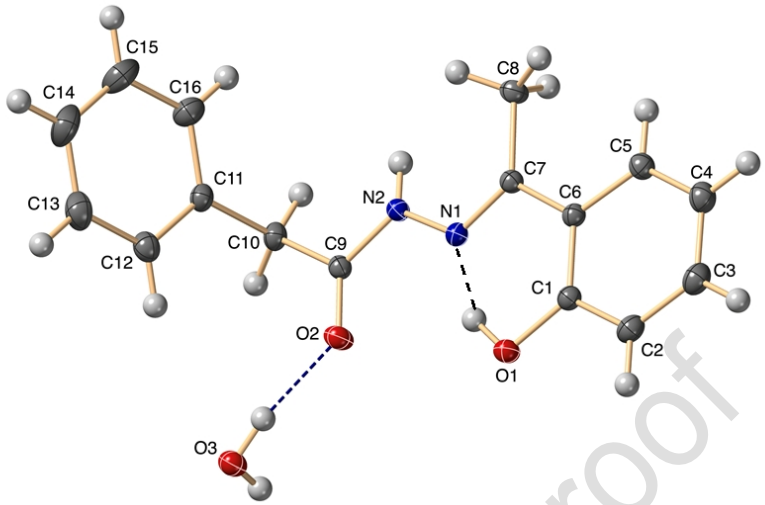

Fig. 3. ORTEP representation of **HL1**

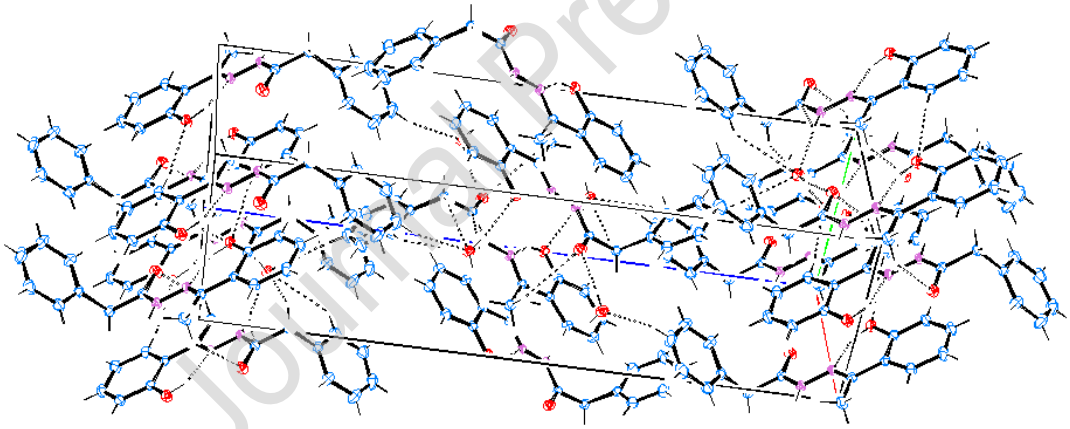

Fig. 4. The unit cell content of **HL1**

The ORTEP representation of the **DIM** molecule is given in **Fig. 5**. As shown from figure, the molecule has the symmetry point group S_2 ($C_2 + \sigma_v$). The two phenyl rings and the C=N-N=C group are planar. The bond distances of the two C=N groups [C(7)-N(1) and C(9)-N(2)] were found to be 1.304 Å and 1.300 Å. These values are slightly longer than that of the parent **HL1** (1.2296 Å). This could be returned to the double-single bond conjugation in the whole molecule. The N(1)-N(2) bond length is slightly longer than that of the parent compound. This enlargement could be due to the existence of two opposite hydrogen bonds (**Fig. 5**). All the other bond lengths

and bond angles are within the normal range of similar compounds. The packing of the **DIM** unit cell shows that the molecules are connected with a net of hydrogen bonding (**Fig. 6**). **Table 3** illustrates the bond separation between H and the donor (D) and the acceptor A as well as the DHA angle.

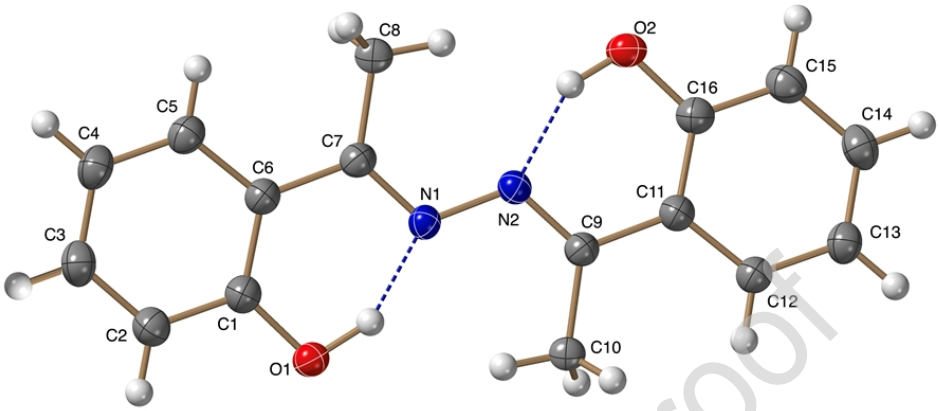

Fig. 5. ORTEP representation of the dimer derivative.

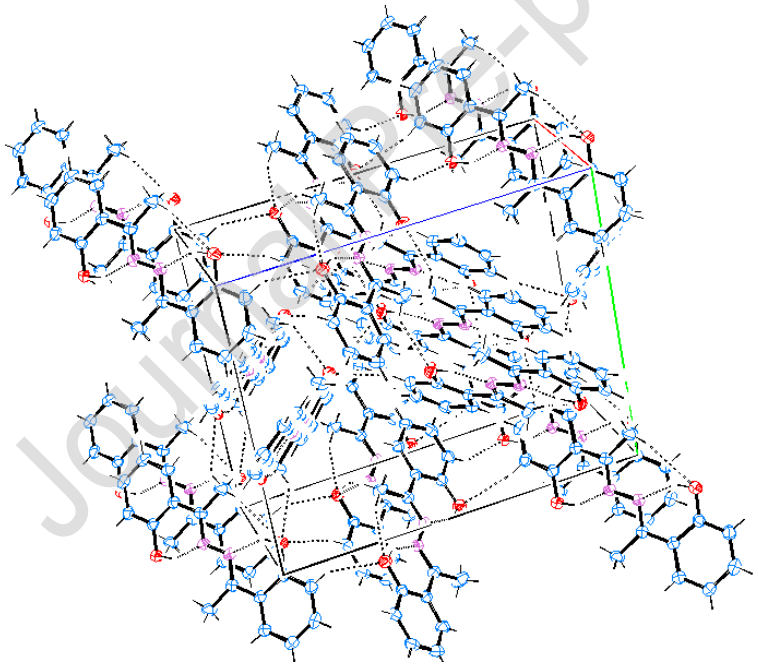

Fig. 6. The unit cell content of the dimer derivative.

The ORTEP diagram (**Fig. 7)** of the binuclear copper complex **[(CuL1)$_2$]** showed that two ligands coordinated as tridentate (two oxygen and one nitrogen) to form five- and six-membered chelates with two Cu ions. It is obvious from the figure that the complex has the symmetry point group S_2 ($C_2 + \sigma_v$). The copper atom is occurred in a distorted square planar coordination geometry.

The distortion in the complex could be illustrated from the bond lengths of Cu-O and Cu-N (1.898 Å, 1.909 Å, 1.934 Å and 1.998 Å) as well as from the bond angles around the Cu ion, which showed significant deviations from 90° [39,40]. Important bond lengths and bond angles are given in **Table 2**. The bond length of C(9)-O(2) for carbonyl group in the complex was enlarged (1.292 Å) relative to that of the ligand (1.2296 Å). This increase in the complex indicated the decrease of the bond order. These data are in consistent with the IR spectra of the two molecules. (The stretching vibration frequency of CO group in the complex was shifted to lower frequency. Further, the change in bond length of C=N between the complex and ligand is consistent with complex formation.

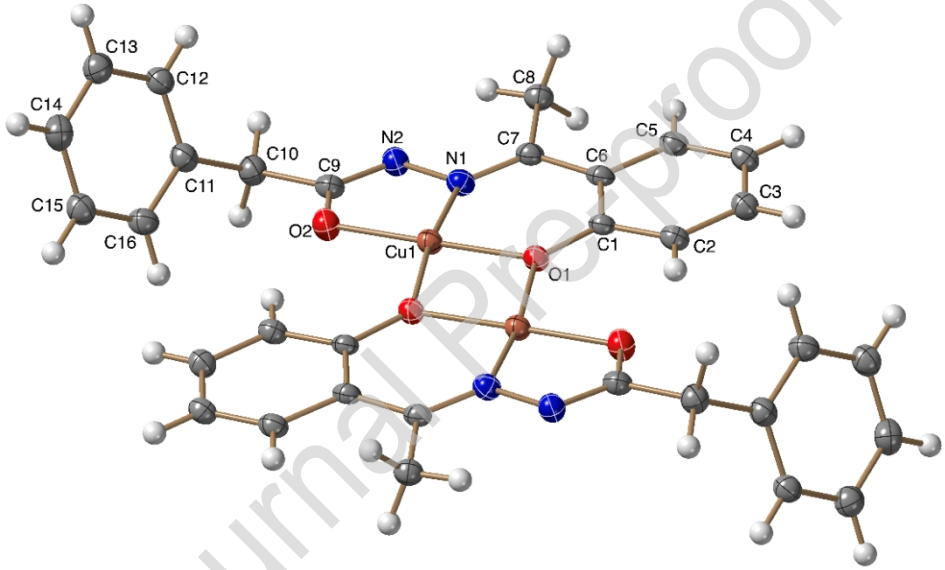

Fig. 7. ORTEP representation of the **[(CuL1)$_2$]** complex.

3.3. Molecular Orbital Calculations

The optimized geometrical parameters, natural charges on active centers, natural configuration of the metal ions and energetics of the ground state for the reported compounds were calculated at the B3LYP/GENECP level. The two ligands (**HL1** and **HL2**) were expected to exist in solution in two geometrical structures, namely the keto- and enol-form. According to the spectroscopic studies, it was found that this was the case for **HL2**, while **HL1** existed in the keto-form only (**Scheme 1**). However, both the two structures (keto/enol) were considered for optimization using the B3LYP/6-311G** level of theory (**Fig. 8**). The energetics of the two ligands and natural charges are listed in **Table 4**. The data indicated that in both ligands, the keto- form is

more stable than the enol-form by about 12 kcal mol^{-1} as reflected from the computed total energy. Obviously, the natural charges computed from NBO analysis showed that the most negative centers for chelation in the two ligands are the two oxygen and adjacent nitrogen atoms.

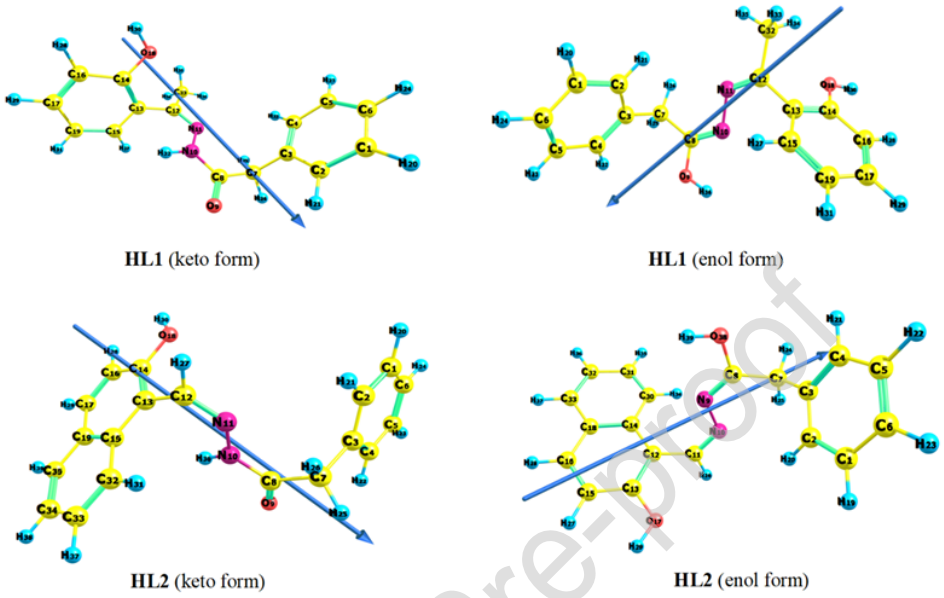

Fig. 8. The optimized geometry of the ligands.

The optimized geometry, numbering system, vector of dipole moment, bond lengths, and bond angles of the two copper complexes are presented in **Fig. 9**. In the two complexes, **$[(CuL1)_2]$** and **$[(CuL2)_2]$**, each copper ion coordinated to one ligand forming a five-and six-membered rings with a distorted square planer arrangement including the two copper ions. The computed M-N and M-O bond lengths showed elongation upon complexation, as observed in the X-ray measurements for **$[(CuL1)_2]$** complex, **Table 2**. These bond lengths are excessively long compared to the typical MX (X = O or N) bond lengths [41]. This could be due to the formation of a binuclear derivatives. The calculated bond angles were found to be in good agreement with the X-ray measurements of **$[(CuL1)_2]$**. The bond angles between the metal ion and binding sites in the coordination sphere vary between 80° and 104°. The computed dihedral angles around the metal ion in the coordination sphere were far from 0° or 180°, which revealed that the metal ion is not in the same plane as the donating sites and the rest of the ligand, i.e. the complexes are non-planar.

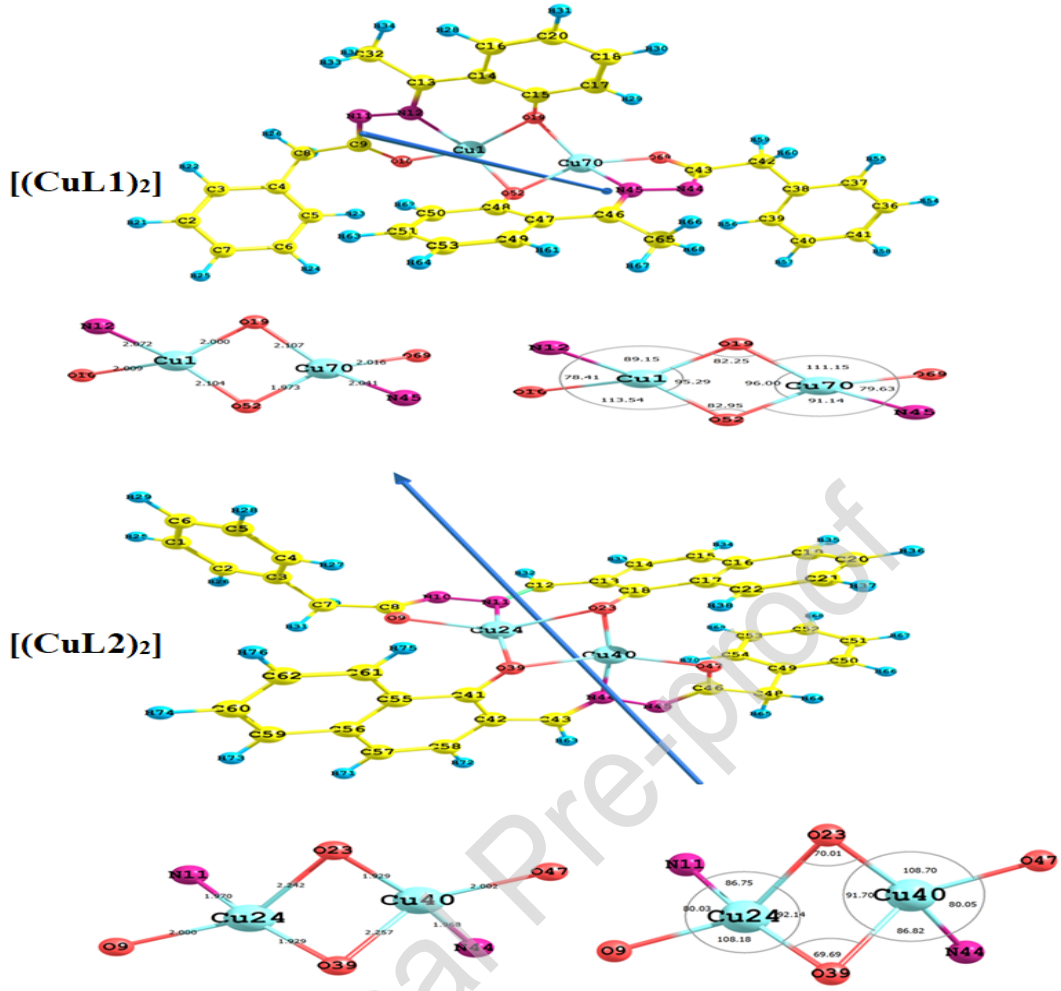

Fig. 9. The optimized geometry, vector of the dipole moment, bond lengths and bond angles of the coordinated center of the copper complexes.

3.3.1. Natural charge and natural population

The accretion of charges on the individual atoms coordinated with the metal ion before and after complexation, the natural population of the electrons of each metal ion in the core, valence and Rydberg sub-shells and natural electronic configuration of the metal ions in the coordination globe of the studied complexes are presented in **Tables 5** and **6**. The most electronegative charges are accumulated on O9, O18 and N11 atoms of the ligands and the complexes. These electronegative atoms in the coordination sphere have a tendency to provide electrons to the central metal ions. The most electropositive charges accrued on the Cu species. Such atoms are more likely to receive electrons from the ligands. In **[(CuL1)$_2$]** complex, one of the Cu central metal ion receives 1.2298e from the ligand with $3d^{9.65}$ configuration, while the other Cu metal ion receives

1.2282e with $3d^{9.64}$ configuration. In case of **[(CuL2)$_2$]** complex, the two Cu central metal ions receive 1.3116e and 1.3159e from the ligand with $3d^{9.66}$ and $3d^{9.65}$ configurations (**Table 5**).

3.3.2. Quantum global reactivity descriptors

The global properties of the reported compounds, HOMO and LUMO, energy gap (*Eg*), chemical hardness (η), electronegativity (χ), chemical potential (V), electron affinity (A), ionization potential (I) and chemical softness (S) were computed and presented in **Table 7**. The donating, E_{HOMO}, and accepting properties, E_{LUMO}, of the studied complexes follow the order: **[(CuL1)$_2$]** > **[(CuL2)$_2$]**. The energy gap (*Eg*) between HOMO and LUMO of the studied complexes characterizes the molecular chemical stability (reactivity). The results shown in **Fig. 10** indicate that the smaller the energy gap the easier the charge transfer and polarization within the molecule. The order of increasing reactivity, also, follow the above order. From the HOMO and LUMO energies, ionization potential and electron affinity are expressed as $I \sim -E_{HOMO}$ and $A \sim -E_{LUMO}$. The variation of electronegativity (χ) values is sustained by electrostatic potential. The results in **Table 7** show that the order of decreasing χ (increasing charge transfer within the complexes) is **[(CuL1)$_2$]** < **[(CuL2)$_2$]**. The small η values for the complexes imitate the ability of charge transfer inside the complexes. The order of increasing charge transfer within the complexes is **[(CuL1)$_2$]** > **[(CuL2)$_2$]**.

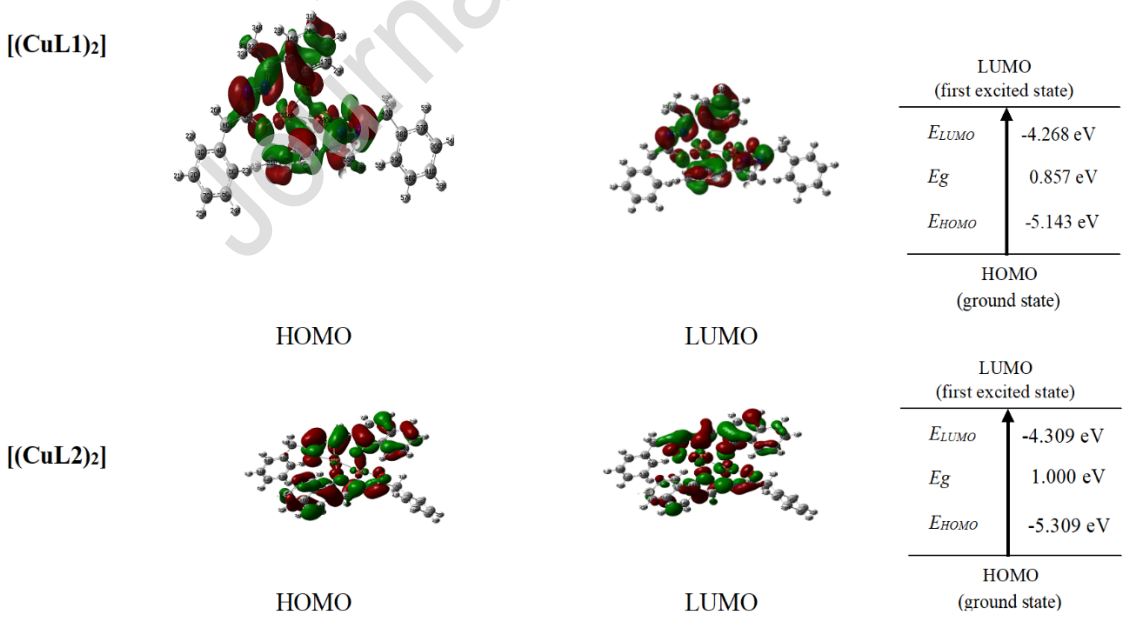

Fig. 10. The HOMO-LUMO charge density maps of the two copper complexes.

3.3.3. Non-quantum global reactivity descriptors

The calculation data of the physicochemical properties of the ligands and complexes are tabulated in **Table 8**. The properties considered are: molar volume (*MV*), hydration energy (*HE*), molar refractivity (*MR*), surface area grid (*SAG*) and polarizability (*Pol*). The calculations were performed using Hyper Chem 8.0.7. The capacity of the electronic system of a molecule to modulate itself upon the application of external electric field of light defines its molecular polarizability (*Pol*) characteristics. Molecular polarizability depends only on the molecular volume, which determines the transport characteristics of molecules. In biology, for example, it includes blood-brain barrier penetration and intestinal absorption [42]. Therefore, modeling of molecular properties and biological activity requires the use of molecular volume in the quantitative structure-activity relationship (QSAR) studies. The molar refractivity (*MR*) is a steric parameter that depends on the spatial array of the aromatic ring in the molecules considered. The importance of the spatial arrangement stems from the fact that it is essential to study the interaction of the drug molecules with the receptor [43]. In addition to the dependence of *MR* on the molecular volume, it also depends on the London dispersive forces that play a strong role in the drug molecules-receptor interaction. **Table 8** illustrates that polarizability data, molecular refractivity and surface area grid are generally proportional to the size and the molecular weight of the studied complexes. Also, the data in the table shows that an increase in the hydrophobic values would result in a decrease in the hydration energy. The change in the values of the hydration energy is affected by the increase or the decrease in the number of hydrogen bonds between donor and acceptor [44].

3.3.4. Non-linear optical properties

To investigate the relationship between molecular structure and non-linear optical (NLO) properties, the polarizabilities and hyperpolarizabilities of the studied complexes were calculated using B3LYP/GENECP method. Total static dipole moment (μ), mean polarizability (α), anisotropy of polarizability ($\Delta\alpha$), mean first-order hyperpolarizability (β), the Hyper-Rayleigh Scattering (β_{HRS}) and the depolarization ratio (*DR*) of the ligands and complexes are listed in **Table 9**. The polarizabilities and first-order hyperpolarizabilities are reported in atomic units (au); the calculated values have been converted into electrostatic units (esu) using conversion factors of 0.1482×10^{-24} esu for α and 8.6393×10^{-33} esu for β. Urea is used as a standard prototype in NLO studies [45]. The magnitude of β is one of the key factors in a NLO system. The analysis of β

computed theoretically for the ligands and complexes shows that the **[(CuL1)$_2$]** complex is 5 times greater than urea, whereas, **[(CuL2)$_2$]** complex is 7 times greater than urea which confirm that all complexes are effective NLO candidates.

3.4. Thermal analysis

The thermogravimetric (TG) studies of the two copper complexes were carried out to give more insight into their thermal properties. The thermal decomposition data of the reported complexes are given in **Table 10**. The mass loss obtained from the TG curves are in good agreement with the calculated values and consistent with the proposed structures. The TG plot of **[(CuL1)$_2$]** complex displayed two decomposition steps within the temperature range 120-800 ^{o}C. The first step with a temperature range of 120-371 ^{o}C corresponded to loss of $C_{15}H_{16}N_2O_2$ moieties, with a mass loss of 38.44 %. The second decomposition step occurred at 374-799 ^{o}C has been assigned to the elimination of $C_{17}H_{12}N_2O_2$ fragments with mass loss of 42.08 % to give finally metallic copper residue.

The TG curve of **[(CuL2)$_2$]** complex exhibited three decomposition steps within the temperature range 125-1000 ^{o}C. The first decomposition step extended from 125 to 249 ^{o}C and referred to the loss of $C_4H_7N_2O$ species with a mass loss of 12.60%. The second step at temperature range 249-349 ^{o}C exhibited a mass loss of 40.73 % and corresponded to the loss of $C_{20}H_{12}N_2O$ moieties. The third decomposition step at temperature range 347-1000 ^{o}C exhibited a mass loss of 37.63 % and may be due to loss of $C_{14}H_9O_2$ fragments leaving a metallic solid residue, **Table 10**.

3.5. Biological activity studies

3.5.1. Antimicrobial activity

In this work, the *in vitro* antimicrobial activities of the two ligands and their copper complexes were screened against two bacteria, *E. coli* and *S. aureus*, and the two fungi, *A. flavus* and *C. albicans*, and compared with the known antibiotics: ampicillin as an antibacterial agent and amphotericin B as an antifungal drug. Unfortunately, the two ligands showed no activity towards either the bacteria or the fungi. On the other hand, the results indicated high antimicrobial activities for the complexes and were found to be comparable with that of standards (**Table 11**). Accordingly, it could be concluded that the Cu ions improved the antimicrobial activity of the compounds. The high activities of the complexes can be explained by the cell permeability concept and/or Tweedy's chelation theory [46-48]. According to the cell permeability concept, the metal

ions can hardly pass through the membrane surrounding the cell due to the high polarity of such ions. On chelation, the polarity of the Cu(II) ions can be reduced to a greater extent as a result of the overlap of the ligand and metal ion orbitals leading to a partial sharing of the positive charge of the metal ion with donor groups. Furthermore, the lipophilicity of complexes is improved as the π-electron delocalization over the whole chelating ring increases. Subsequently, the penetration of the complexes into lipid membranes will be enhanced and then blocking the Cu(II) binding sites in the enzymes of microorganisms.

3.5.2. Antioxidant activities by DPPH radical scavenging activity

Antioxidants have capacity to protect organisms and cells from damage caused by oxidative stress during metabolism. It is well known that free radical oxidative processes play a significant pathological role in causing many human diseases together with aging [49]. The DPPH˙ has been widely used for free radical-scavenging assessments due to its ease and convenience. *In vitro* antioxidant activity of the two copper complexes was evaluated by DPPH free radical scavenging method. The antioxidant property of the tested samples was evaluated at different concentrations (25, 50, 100, 150 and 200 μg/mL), and ascorbic acid was used as a standard for the comparison. The percent DPPH˙ scavenging values at 30 min incubation time are given in **Fig. 11**. For the activity comparison of the complexes, it was observed that the antioxidant activity increased with increasing the concentration. As shown from figure, the percent DPPH˙ scavenging activity of the two complexes are higher than the standard ascorbic acid until the value 100 μM. The activity of the standard then increases relative to the complexes at higher concentrations. Also, the data showed that **[(CuL1)$_2$]** complex has more potent antioxidant activity with the lowest IC_{50} value (42.3 μg/mL) relative to **[(CuL2)$_2$]** complex (50.1 μg/mL) and the standard (84.2 μg/mL).

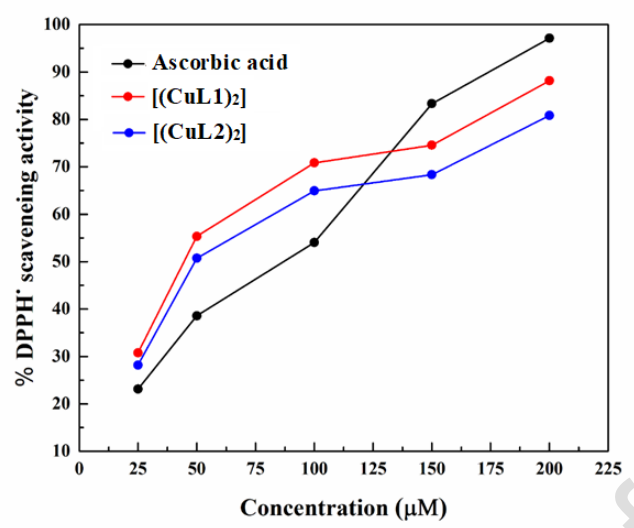

Fig. 11. The % DPPH˙ radical scavenging activities of the Cu complexes and ascorbic acid.

3.5.3. Fluorescence quenching studies

Fluorescence spectroscopy technique is used technique to study the interactions between small molecules and DNA [50-52]. Ethidium bromide (EB) was used to investigate the potential DNA binding mode of the reported copper complexes. EB emits intense fluorescence at 608 nm in the presence of CT-DNA due to its strong intercalation between the adjacent DNA base pairs. The addition of a second molecule which binds to DNA more strongly than EB would quench the DNA-induced EB emission [49]. The extent of quenching of the fluorescence of EB bound to DNA would reflect the extent of the DNA binding of the second molecule. The emission spectra of DNA-bound EB in the absence and the presence of different concentrations of the Cu complexes are shown in **Fig. 12**. It is clearly seen that the addition of the Cu complexes to CT-DNA pretreated with EB caused an appreciable reduction in emission intensity, indicating that the complexes bind to DNA at the sites occupied by EB. It is evident that the replacement of EB bound to DNA results in a decrease in fluorescence intensity with the increase in concentration of the investigated compounds. This implies that the complexes can strongly compete with EB in binding to DNA. Fluorescence quenching can occur by different mechanisms, which are usually classified as dynamic and static quenching. The former results from collision between the quencher and the fluorophore, while the latter is due to the formation of a complex between the fluorophore and quencher [53]. The K_{SV} values were obtained from the slope of the linear plot of I_o/I versus [Q], **Fig. 13**. The figure illustrate that the quenching of EB bound to CT-DNA by Cu complexes are in

good agreement with the linear Stern-Volmer equation. The K_{SV} values were 2.25 x10^4 and 5.51x10^4 for the **[(CuL1)$_2$]** and **[(CuL2)$_2$]**, respectively.

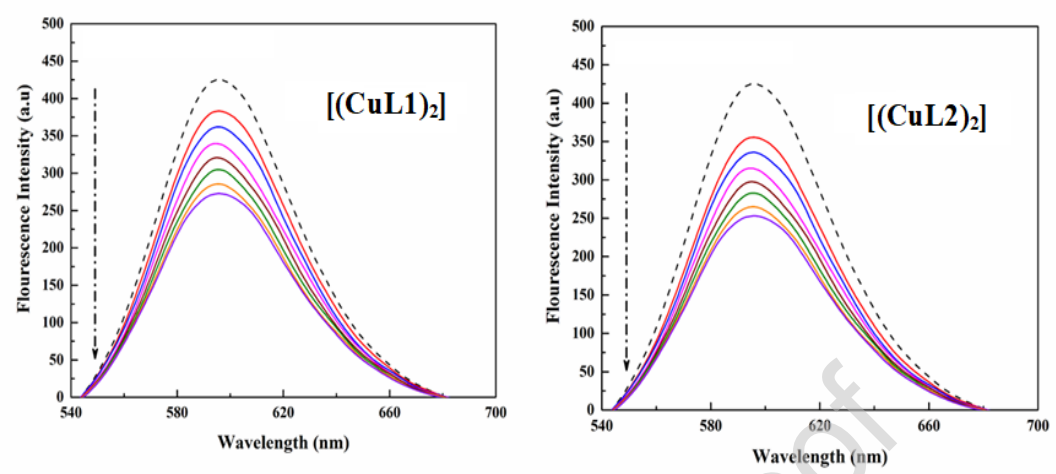

Fig. 12. Fluorescence emission spectra of the EB-DNA system (1×10^{-5} M, 1:1) in absence (dashed line) and presence (solid line) of copper complex (1.0-8.0×10^{-5} M). The arrow indicates the intensity changes upon increasing concentration of the complex.

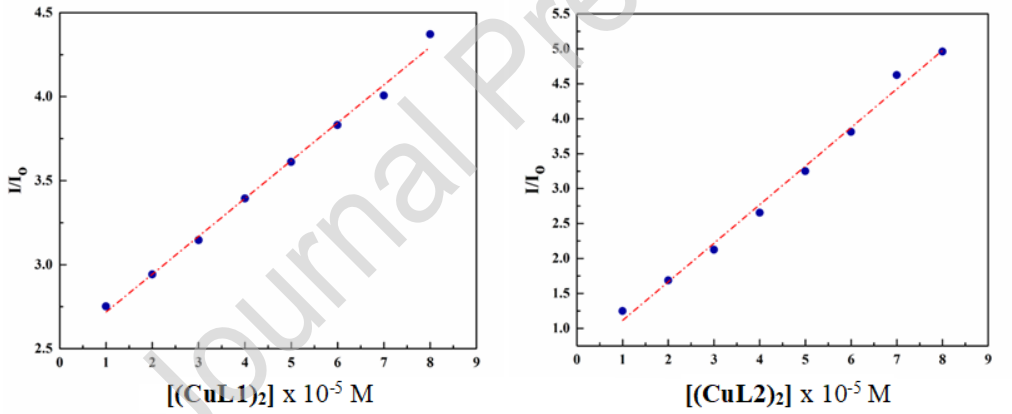

Fig. 13. Fluorescence variation profiles of the two copper complexes versus molar concentrations.

3.5.4. Viscosity measurements

Optical or photophysical probes generally provide necessary, but not sufficient clues to support an intercalative binding models [54]. The viscosity studies provide a strong evidence for mode of binding. To identify the intercalative binding, viscosity experiments were performed. Intercalating agents are expected to increase the relative specific viscosity of CT-DNA due to elongation of the double helix to accommodate the compounds in between the base pairs. In

contrast, a partial and/or non-classical intercalation may bend (or kink) DNA helix, under the same conditions, typically results in less pronounced effect on its effective length and its viscosity [55]. The plots of relative viscosity $(\eta/\eta_o)^{1/3}$ versus R, R = [Cu Complex]/[DNA], showed a significant increase in the relative specific viscosity of DNA solution with increasing concentration of complexes, **Fig. 14**. This indicates that complexes bind to CT-DNA through an intercalation binding mode [56]. Such behavior is consistent with other intercalates (i.e., EB), which increase the relative specific viscosity for the lengthening of the DNA double helix resulting from intercalation. The results clearly indicate that the complexes intercalate between adjacent base pairs, which is in agreement with the other experimental results. The increased degree of viscosity, which may depend on its affinity to DNA, follows the order of **$[(CuL2)_2]$** > **$[(CuL1)_2]$**, which is consistent with the foregoing hypothesis suggested from fluorescence quenching data. The increased in degree of viscosity showed that changing the metal environment can modulate the binding property of the complex with DNA. The results of DNA binding studies indicated, that the suggested mechanism for interaction between the compounds and DNA was via an intercalative mode.

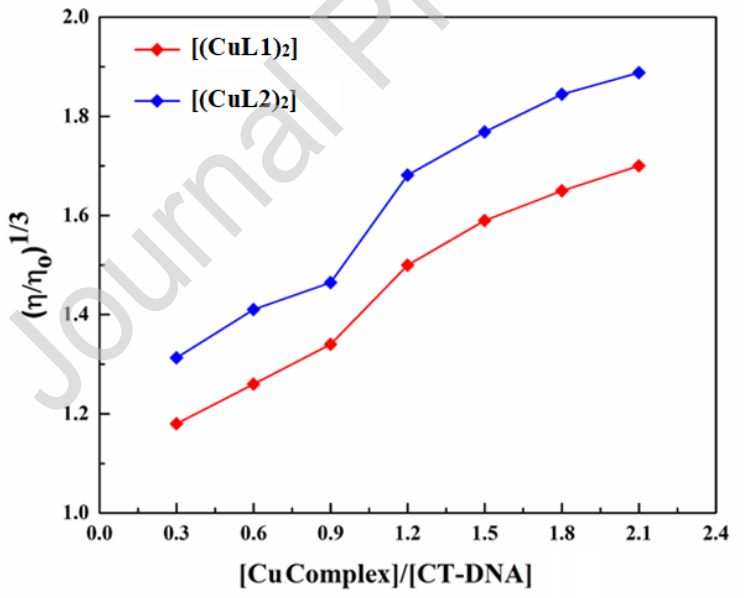

Fig. 14. Effect of increasing concentrations of the Cu complexes on the relative viscosity of CT-DNA at 30 ± 0.1 °C

3.6. Molecular docking of the ligands and ***$[(CuL2)_2]$*** *complex*

Molecular docking is a great approach to understand the interaction between the synthesized compounds and biological target. Analysis of the docking data is useful in predicting the conformational changes associated with the amino acid residues at the binding position to accommodate the docked hydrophobic inhibitors. The two ligands **HL1** and **HL2** and the **[(CuL2)$_2$]** complex, as an example, were subjected to molecular docking studies using the MOE version 2016.08 to understand the compound-DNA interactions and to explore the potential binding mode and energy. The docked ligands conformations were rated according to the binding energy, hydrogen bonding and hydrophobic interactions between the ligands and the copper complex, and the B-DNA (PDB ID:1BNA). The docking studies determine the way by which the docked compounds fundamentally fit in the DNA minor groove and comprise of hydrophobic, ionic, and hydrogen bonding interactions with the DNA bases. It was found that the most of the optimal docking results were in the GC region. These theoretical studies support the expeimental findings of the fluorescence quenching and viscosity measurements, which indicated the intercalative mode for DNA interaction. The binding interactions of the two ligands and the **[(CuL2)$_2$]** complex are displayed in **Figs. 15-17**. The free ligands **HL1** and **HL2** showed very good binding scores with high negative e-values, which represent high binding affinity between the receptor and ligand molecules indicating the higher efficiency of the bioactive compounds (-5.3551 and -6.0999 kcal/mol for **HL1** and **HL2**, respectively). In case of **HL1**, the binding interaction comes from hydrophobic interaction between the amino acid residues such as DA 18, DC 15 and DG 16 with the aromatic moiety of the ligand. On the other hand, the binding interaction of **HL2** comes from the hydrogen bonds formed between DG16 and the OH group of ligand, interaction of DA18 with the phenyl moiety and the hydrogen bonds formed between water molecules and the NH group of **HL2**. In case of the **[(CuL2)$_2$]** complex, it exhibits the best binding score of -6.6479 kcal/mol with four hydrogen bonds to DNA, **Fig. 17**. Thus, it is clear that these bioactive compounds were able to interact with the available binding sites of the target proteins effectively. The order of increasing of binding interaction is as follows: **HL1** < **HL2** < **[(CuL2)$_2$]**.

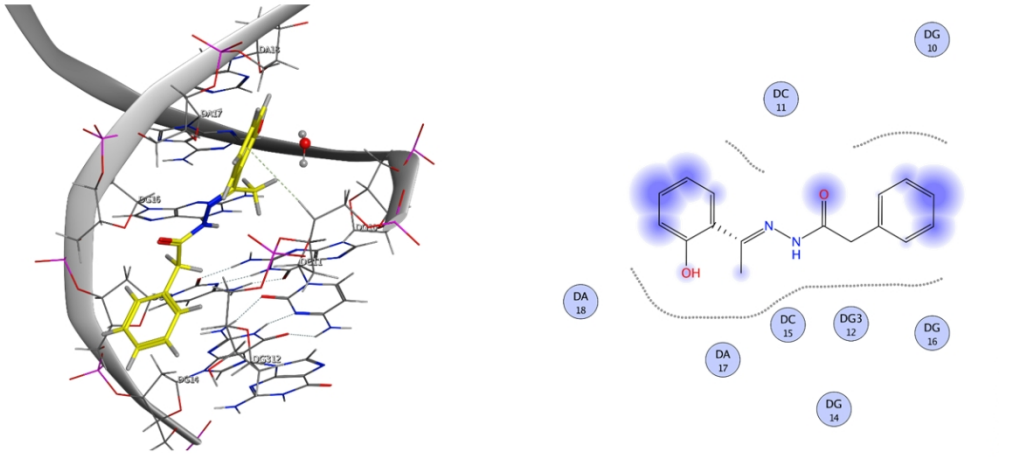

Fig. 15. 3D and corresponding 2D representation of **HL1** interaction with DNA.

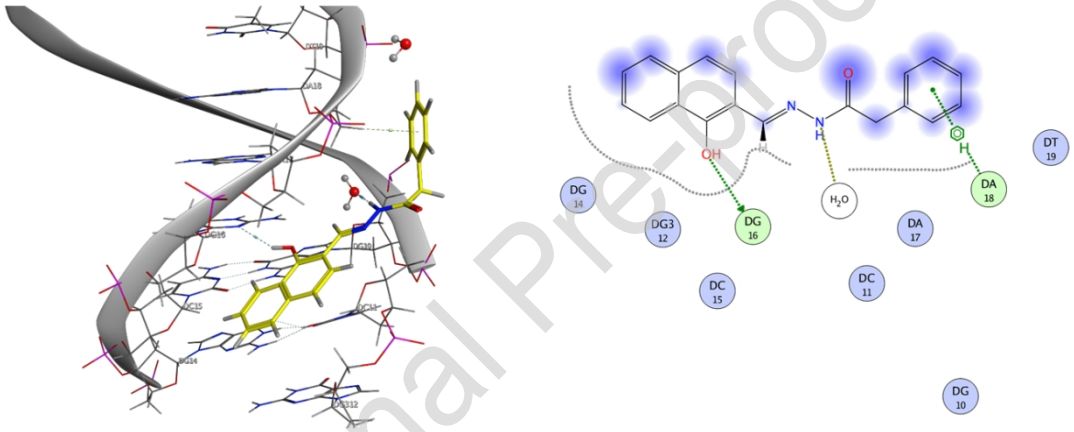

Fig. 16. 3D and corresponding 2D representation of **HL2** interaction with DNA.

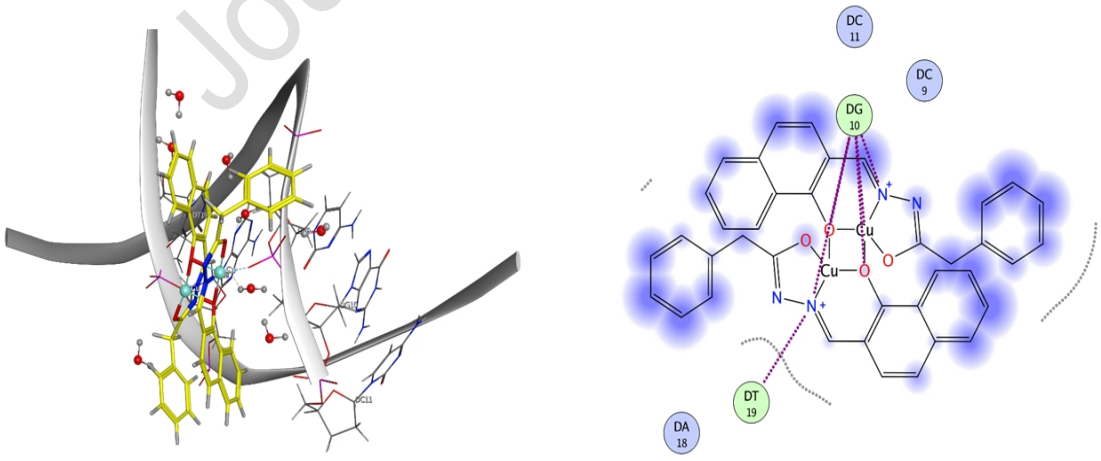

Fig. 17. 3D and corresponding 2D representation of **[(CuL2)$_2$]** interaction with DNA.

4. Conclusion

The two Schiff bases, **HL1** and **HL2**, and their binuclear copper complexes were found to have interesting spectroscopic and structural features. Acid catalyzed reaction of **HL1** gave a dimer that probably formed via radical mechanism. The molecular geometries of the ligands and their complexes in the ground state, calculated by DFT, showed that the optimized structures of the compounds are nonlinear as reflected from the X-ray analysis. The reactivity of the copper complexes were stemmed from the quantum and non-quantum global parameters. The dipole moment and hyperpolarizability data indicated that the complexes have a reasonably good NLO behavior. Biological activities, fluorescence quenching, viscosity measurements and molecular docking studies supported and indicated that the ligands and their copper complexes have the ability to bind with DNA. Copper complexes have more ability to interact with DNA than the free ligands. The complexes may, therefore, be promising potential drugs for therapeutic intervention in various diseases.

Supplementary data

Files containing complete date for the crystal structures have been submitted to the Cambridge Crystallographic Data Center with reference numbers CCDC deposition no. 1908713 (**HL1**), 1880656 (**[(CuL1)$_2$]**) and 1940696 (**DIM**).

References

[1] L.H. Abdel-Rahman, N.M. Ismail, M. Ismael, A.M. Abu-Dief, E.A. Ahmed, J. Mol. Struct. 1134 (2017) 851-862. https://doi.org/10.1016/j.molstruc.2017.01.036

[2] R.G. Mohamed, A.A. Makhlouf, S.A. Mosad, A.A. Abdel Aziz, S.M. El-Medani, R.M. Ramadan, J. Coord. Chem. 71, (2018) 3665-3688. https://doi.org/10.1080/00958972.2018.1526375

[3] X. W. Zhu, Russ. J. Coord. Chem. 45 (2019) 532-538. https://doi.org/10.1134/S1070328419070091

[4] A. Jayamani, N. Sengottuvelan, S. K. Kang, Y-I. Kim, Inorg. Chem. Commun. 48 (2014) 147-152. http://dx.doi.org/10.1016/j.inoche.2014.08.029

[5] D. Ma, L. Zhang, X. Rao, T. Wu, D. Li, X. Xie, J. Coord. Chem. 66 (2013) 1486-1496. https://doi.org/10.1080/00958972.2013.783699

[6] F.A. Beckford, J. Thessing, M. Shaloski Jr, P.C. Mbarushimana, A. Brock, J. Didion, J. Woods, A. Gonzalez-Sarrías, N. P. Seeram, J. Mol. Struct. 992 (2011) 39-47. DOI: 10.1016/j.molstruc.2011.02.029

[7] L. Yan, Z. Zhi-gang, International Conference on Electronic Science and Automation Control, (2015). https://doi.org/10.2991/esac-15.2015.1

[8] N. Vamsikrishna, M.P. Kumar, S. Tejaswi, A. Rambabu, Shivaraj. J. Fluoresc. 26, (2016) 1317-1329. doi: 10.1007/s10895-016-1818-z

[9] P. Subbaraj, A. Ramu, N. Raman, J. Dharmaraja, Spectrochim. Acta, A, 117 (2014) 65-71. https://doi.org/10.1016/j.saa.2013.07.096

[10] P. Kumar, B. Narasimhan, Mini Rev. Med. Chem. 13 (2013) 971-987.

[11] V. Angelova, V. Karabeliov, P.A. Andreeva-Gateva, J. Tchekalarova, Drug Dev. Res. 77 (2016) 379-392. doi: 10.1002/ddr.21329

[12] G. Verma, A. Marella, M. Shaquiquzzaman, M. Akhtar, M.R. Ali, M.M. Alam, J. Pharm. BioAllied Sci. 6 (2014) 69-80. doi: 10.4103/0975-7406.129170

[13] R. Kaplánek, M. Jakubek, J. Rak, Z. Kejík, M. Havlík, B. Dolenský, I. Frydrych, M. Hajdúch, M. Kolář, K. Bogdanová, J. Králová, P. Džubák, V. Král, Bioorg. Chem. 60 (2015)19-29. https://doi.org/10.1016/j.bioorg.2015.03.003

[14] M. Bingul, O. Tan, C.R. Gardner, S.K. Sutton, G.M. Arndt, G.M. Marshall, B.B. Cheung, N. Kumar, D.S. Black, Molecules 21 (2016) E916. doi: 10.3390/molecules21070916

[15] B. Kocyigit-Kaymakcioglu, S.S. Yazici, F. Tok, M. Dikmen, S. Engür, E.E. Oruc-Emre, A. Iyidogan, Letters in Drug Design & Discovery, 16 (2019) 522-532. https://doi.org/10.2174/1570180815666180816124102

[16] R.P. Bakale, G.N. Naik, C.V. Mangannavar, I.S. Muchchandi, I.N. Shcherbakov, C. Frampton, K.B. Gudasi, Eur. J. Med. Chem. 73 (2014) 38-45. doi: 10.1016/j.ejmech.2013.11.037

[17] a) H-Q. Chang, L. Jia, J. Xu, W-N. Wu, T-F. Zhu, R-H. Chen, T-L. Ma, Y. Wang, Z-Q. Xu, Trans. Met. Chem. 40 (2015) 485-491. https://doi.org/10.1007/s11243-015-9938-x. b) D. Gewirth, An Oscillation Data Processing Suite for acromol. Cryst, 6th ed., 2003.

[18] a) C. Marzano, M. Pellei, F. Tisato, C. Santini, Anti-Cancer Agents in Medicinal Chemistry, 2009, 9, 185-211. DOI: 10.2174/187152009787313837. b) I. Iakovidis, I. Delimaris, S.M. Piperakis, Molecular Biology International, 2011 (2011), Article ID 594529. doi:10.4061/2011/594529

[19] G.M. Sheldrick, SADABS e Bruker AXS Scaling and Absorption Correction, Bruker AXS, Inc, Madison, Wisconsin, USA, 2012.

[20] G.M. Sheldrick, Acta Cryst. A64 (2008) 112-122. https://doi.org/10.1107/S0108767307043930

[21] E.F. Pettersen, T.D. Goddard, C.C. Huang, G.S. Couch, D.M. Greenblatt, E.C. Meng, J. Comput. Chem. 25 (2004) 1605-1612. DOI 10.1002/jcc.20084

[22] L.J. Barbour, J. Supramol. Chem. 1 (2001) 189-191. https://doi.org/10.1016/S1472-7862(02)00030-8

[23] Z. Otwinowski, W. Minor, Methods in Enzymology, 276 (1997) 307-326. https://doi.org/10.1016/S0076-6879(97)76066-X

[24] D. Avci, Spectrochim. Acta A, 82 (2011) 37-43. https://doi.org/10.1016/j.saa.2011.06.037

[25] Y. Ünver, K. Sancak, F. Çelik, E. Birinci, M. Küçük, S. Soylu, N. A. Burnaz, Eur. J. Med. Chem. 84 (2014) 639-650. doi: 10.1016/j.ejmech.2014.01.014

[26] T.F. Tullis, Metal-DNA chemistry, ACS Symposium Series, Vol. 402, American Chemical Society, Washington DC, USA, 1989.

[27] M.J. Waring, J. Mol. Biol. 13 (1965) 269-282. https://doi.org/10.1016/S0022-2836(65)80096-1

[28] J. Gunjan and D. Awadh, Int. Res. J. Pharm. 2 (2011) 110-112.

[29] R.M. Ramadan, A.K. Abu Al-Nasr, A.F.H. Noureldeen, Spectrochim. Acta A, 132 (2014) 417-422. https://doi.org/10.1016/j.saa.2014.04.151

[30] R.M. Ramadan, M.S.A. Hamza, A.S. Attia, Polyhedron, 16 (1997) 229-233. https://doi.org/10.1016/0277-5387(96)00278-1

[31] R.M. Claramunt, C. Lopez, M.D. Santa Maria, D. Sanz, J. Elguero, Prog. Nucl. Mag. Reson. Spec. 49 (2006) 169-206. DOI: 10.1002/chin.200711279

[32] M.M.H. Khalil, M.M. Aboaly, R. M. Ramadan, Spectrochim. Acta A, 61 (2005) 157-161. https://doi.org/10.1016/j.saa.2004.03.015

[33] K. Nakamoto, Infrared and Raman Spectra of Inorganic and Coordination Compounds, part B, 6th ed., John Wiley & Sons, Inc., Hoboken, New Jersey, 2009.

[34] D. Kivelson, R. Neiman, J. Chem. Phys. 35 (1961) 149-155. https://doi.org/10.1063/1.1731880

[35] L.H. Abdel-Rahman, R. M. Ramadan, J. Coord. Chem. 60 (2007) 1891-1901. https://doi.org/10.1080/00958970701209864

[36] S. Chandra, K. Gupta. Trans. Met. Chem. 27 (2002) 329-332. https://doi.org/10.1023/A:101489870

[37] A. Sankaraperumal, J. Karthikeyan, A.N. Shetty, R. Lakshmisundaram, Polyhedron, 50 (2013) 264-269. https://doi.org/10.1016/j.poly.2012.11.006

[38] E.A. El-Samanody, Appl. Organometal. Chem. 32 (2018), e4586. DOI: 10.1002/aoc.4586

[39] R.M. Ramadan, S.M. Shohayeb, R.G. Mohamed, Synth. React. Inorg. Met.-Org. Nano-Met. Chem. 43 (2013) 609-616. https://doi.org/10.1080/15533174.2012.752390

[40] J.T. Brewster, G. Anguera, M.D. Moore, B.S. Dolinar, H. Zafar, G.D. Thiabaud, V.M. Lynch, S.M. Humphrey, J.L. Sessler, Inorg. Chem. 56 (2017) 12665-12669. doi: 10.1021/acs.inorgchem.7b01669

[41] L. Armelao, S. Quici, F. Brigelletti, G. Accorsi, G. Bottaroi, M. Cavazzini, E. Tendello, Coord. Chem. Rev. 254 (2010) 487-505. https://doi.org/10.1016/j.ccr.2009.07.025

[42] J. Wang, X.-Q. Xie, T. Hou, X. Xu, J. Phys. Chem. A, 111 (2007) 4443-4448. https://doi.org/10.1021/jp068423w

[43] P.P. Kapupara, C.R. Matholiya, A.S. Dedakiya, T.R. Desai, Int. Bull. Drug Res. 1 (2011) 1-10.

[44] M. Andrasi, P. Buglyo, L. Zekany, A. Gaspar, J. Pharm. Biomed. Anal. 44 (2007) 1040-1047. DOI: 10.1016/j.jpba.2007.04.024

[45] Y.Y. Lin, N. P. Rajesh, P. S. Raghavan, P. Ramasamy, Y. C. Huang, Mater. Lett. 56 (2002) 1074-1077. https://doi.org/10.1016/S0167-577X(02)00680-8

[46] N.A. Smith, P. Zhang, S.E. Greenough, M.D. Horbury, G.J. Clarkson, D. McFeely, A. Habtemariam, L. Salassa, V.G. Stavros, C.G. Dowson, P.J. Sadler, Chem. Sci. 8 (2017) 395-404. DOI: 10.1039/c6sc03028a

[47] D.W. Deamer, A. Kleinzeller, D.M. Fambrough (Eds.), Membrane Permeability: 100 Years since Ernest Overton, Current Topics in Membranes, vol. 48, Academic Press, San Diego, CA, 1999.

[48] B.G. Tweedy, Phytopathology 55 (1964) 910-917.

[49] Z-C. Liu, B-D. Wang, Z-Y. Yang, Y. Li, D-D. Qin, T-R. Li, Eur. J. Med. Chem. 44 (2009) 4477-4484. https://doi.org/10.1016/j.ejmech.2009.06.009

[50] M. Sirajuddin, S. Ali, A. Badshah, J. Photochem. Photobiol. B 124 (2013) 1-19. doi: 10.1016/j.jphotobiol.2013.03.013

[51] P. Sathyadevi, P. Krishnamoorthy, M. Alagesan, K. Thanigaimani, P. Thomas Muthiah, N. Dharmaraj, Polyhedron, 31 (2012) 294-306. https://doi.org/10.1016/j.poly.2011.09.021

[52] J. Zhang, X.J. Wang, Y.J. Yan, W.S. Xiang, J. Agric. Food Chem. 59 (2011) 7506-7513. doi: 10.1021/jf2005194

[53] F. Samari, B. Hemmateenejad, M. Shamsipur, M. Rashidi, H. Samouei, Inorg. Chem. 51 (2012) 3454-3464. doi: 10.1021/ic202141g

[54] L. Jia, P. Jiang, J. Xu, Z.Y. Hao, X.M. Xu, L.H. Chen, J.C. Wu, N. Tang, Q. Wang, J.J. Vittal, Inorg. Chim. Acta, 363 (2010) 855-865. https://doi.org/10.1016/j.ica.2009.12.047

[55] S. Satyanarayana, J.C. Dabrowiak, J. Chaires, Biochem. 32 (1993) 2573-2584. https://doi.org/10.1021/bi00061a015

[56] S. Anbu, M. Kandaswamy, S. Kamalraj, J. Muthumarry, B. Varghese, Dalton Trans. 40 (2011) 7310-7318. doi: 10.1039/c1dt10277j

Table 1. Crystal data and structure refinement for **HL1**, **DIM** and **[(CuL1)$_2$]**.

Identification code	**HL1**	**DIM**	**[CuL1]$_2$**
Empirical formula	C16 H18 N2 O3	C16 H16 N2 O2	C32 H28 Cu2 N4 O4
Formula weight	286.32	268.31	659.66
Temperature	120(2) K	120(2) K	120(2) K
Wavelength	0.71073 Å	1.54184 Å	1.54184 Å
Crystal system	Monoclinic	Orthorhombic	Monoclinic
Space group	$P2_1/n$	$P2_12_12_1$	$P2_1/c$
Unit cell dimensions	a = 6.9402(2) Å b = 8.3068(2) Å c = 25.5335(6) Å α= 90°. β= 95.100(2)°. γ = 90°.	a = 6.2737(2) Å b = 13.3982(4) Å c = 15.9154(5) Å α= 90° β= 90° γ = 90°	a = 15.0750(7) Å b = 4.6151(2) Å c = 18.8312(7) Å α= 90° β= 90.287(4)° γ = 90°
Volume	1466.20(7) Å^3	1337.79(7) Å^3	1310.12(10) Å^3
Z	4	4	2
Density (calculated)	1.297 Mg/m^3	1.332 Mg/m^3	1.672 Mg/m^3
Absorption coefficient	0.091 mm^{-1}	0.718 mm^{-1}	2.403 mm^{-1}
F(000)	608	568	676
Crystal size	0.234 x 0.128 x 0.071 mm^3	0.203 x 0.072 x 0.056 mm^3	0.194 x 0.041 x 0.026 mm^3
Theta range for data collection	2.579 to 36.314°.	4.313 to 77.010°.	2.931 to 77.380°.
Index ranges	-11<=h<=11, -13<=k<=13, -42<=l<=42	-7<=h<=6, -16<=k<=16, -20<=l<=19	-18<=h<=19, -5<=k<=5, -23<=l<=19
Reflections collected	45765	15508	14086
Independent reflections	7089 [R(int) = 0.0465]	2817 [R(int) = 0.0387]	2761 [R(int) = 0.0772]
Completeness to theta = 25.242°	99.7 %	100.0 %	100.0 %
Absorption correction	Analytical	Semi-empirical from equivalents	Semi-empirical from equivalents
Max. and min. transmission	0.994 and 0.985	1.00000 and 0.69745	1.00000 and 0.65653
Refinement method	Full-matrix least-squares on F^2	Full-matrix least-squares on F^2	Full-matrix least-squares on F^2
Data / restraints / parameters	7089 / 0 / 199	2817 / 0 / 191	2761 / 0 / 191
Goodness-of-fit on F^2	1.031	1.048	1.066
Final R indices [I>2sigma(I)]	R1 = 0.0511, wR2 = 0.1289	R1 = 0.0358, wR2 = 0.0974	R1 = 0.0480, wR2 = 0.1240
R indices (all data)	R1 = 0.0781, wR2 = 0.1456	R1 = 0.0414, wR2 = 0.1024	R1 = 0.0625, wR2 = 0.1360
Extinction coefficient	n/a	n/a	n/a
Largest diff. peak and hole	0.471 and -0.259 e.Å^{-3}	0.191 and -0.169 e.Å^{-3}	0.800 and -0.900 e.Å^{-3}

Table 2. Selected bond lengths, bond angles for **HL1**, **DIM** and **[(CuL1)$_2$]**.

Compound	Bond length (Å)		Bond angles (°)	
HL1	O(1)-C(1)	1.3629(12)	O(2)-C(9)-N(2)	122.25(9)
	O(2)-C(9)	1.2296(12)	C(7)-N(1)-N(2)	119.90(8)
	N(1)-C(7)	1.2944(12)	C(9)-N(2)-N(1)	116.94(8)
	N(1)-N(2)	1.3723(11)	O(1)-C(1)-C(6)	122.46(8)
	N(2)-C(9)	1.3545(13)	C(1)-C(6)-C(7)	121.84(8)
	C(9)-C(10)	1.5124(14)	N(1)-C(7)-C(6)	115.38(8)
DIM	O(1)-C(1)	1.351(3)	C(16)-O(2)-H(2)	106(2)
	O(1)-H(1)	1.00(4)	C(7)-N(1)-N(2)	116.31(16)
	O(2)-C(16)	1.351(3)	C(9)-N(2)-N(1)	116.41(16)
	O(2)-H(2)	0.95(4)	O(1)-C(1)-C(2)	117.31(19)
	N(1)-C(7)	1.304(3)	O(1)-C(1)-C(6)	122.11(19)
	N(1)-N(2)	1.387(2)	N(1)-C(7)-C(6)	116.67(17)
	N(2)-C(9)	1.300(3)	N(1)-C(7)-C(8)	123.8(2)
[CuL1]$_2$	Cu(1)-O(2)	1.898(2)	O(2)-Cu(1)-O(1)	176.47(10)
	Cu(1)-O(1)	1.909(2)	O(2)-Cu(1)-N(1)	82.54(11)
	Cu(1)-N(1)	1.934(3)	O(1)-Cu(1)-N(1)	94.24(11)
	O(1)-C(1)	1.355(4)	C(1)-O(1)-Cu(1)	125.8(2)
	O(2)-C(9)	1.292(4)	C(9)-O(2)-Cu(1)	110.5(2)
	N(1)-C(7)	1.297(4)	C(7)-N(1)-Cu(1)	128.8(2)
	N(1)-N(2)	1.408(4)	N(2)-N(1)-Cu(1)	112.9(2)
	N(2)-C(9)	1.313(4)	C(9)-N(2)-N(1)	109.0(3)

Table 3. Hydrogen bonds for **HL1** and **DIM**.

Compound	D-H...A	d(D-H) Å	d(H...A) Å	d(D...A) Å	<(DHA)°
HL1	O(1)-H(1)...N(1)	0.95(2)	1.66(2)	2.5267(11)	151.6(19)
	O(3)-H(3A)...O(2)	0.88	1.85	2.7170(11)	169.0
DIM	O(1)-H(1)...N(1)	1.00(4)	1.62(4)	2.541(2)	151(3)
	O(2)-H(2)...N(2)	0.95(4)	1.68(4)	2.546(2)	150(3)

Table 4. The energetics and partial charge of the active centers of the tautomers of the ligands and their anions.

	HL1 (keto)	**HL1** (enol)	**L1**$^{-}$
$E_{T(au)}$	-879.516	-879.497	-878.978
E_{HOMO}	-0.00289	-0.00046	-0.05072
E_{LUMO}	0.00443	0.00071	0.05822
E_g (ev)	0.1991	0.0318	2.963
O_9	-0.61768	-0.68577	-0.64846
O_{18}	-0.67124	-0.69146	-0.80606
N_{10}	-0.44452	-0.38530	-0.45091
N_{11}	-0.26928	-0.26555	-0.36071
μ, D	5.2484	2.4030	10.596

	HL2 (keto)	**HL2** (enol)	**L2**$^{-}$
E_T	-993.860	-993.841	-993.331
E_{HOMO}	-0.00244	-0.00210	-0.06098
E_{LUMO}	0.00317	0.00442	0.0598
E_g (ev)	0.1525	0.1773	.285
O_9	-0.60912	-0.6639	-0.64616
O_{18}	-0.66570	-0.67749	-0.80601
N_{10}	-0.44647	-0.43254	-0.4146
N_{11}	-0.24720	-0.31322	-0.31956
μ ,D	5.1267	2.5229	5.6785

Table 5. Natural charge, natural population and natural electronic configuration of the central metal ion of the two copper complexes.

	Natural charge	Core	Natural population			Natural Electronic Configuration
			Valence	Rydberg	Total	
[(CuL1)$_2$]						
$Cu_{(1)}L_1$	0.77017	17.99397	10.22786	0.00799	28.22983	[core]4s(0.27) 3d(9.65) 4p(0.31) 5p(0.01)
$Cu_{(70)}L_1$	0.76187	17.99389	10.22588	0.00835	28.23813	[core]4s(0.27) 3d(9.64) 4p(0.33) 5p(0.01)
[(CuL2)$_2$]						
$Cu_{(24)}L_2$	0.68841	17.98988	10.31142	0.01028	28.31159	[core]4s(0.31) 3d(9.66) 4p(0.35) 5p(0.01)
$Cu_{(40)}L_2$	0.68408	17.98985	10.31453	0.01155	28.31592	[core]4s(0.35) 3d(9.65) 4p(0.35) 5p(0.01)

Table 6. Natural charges of the coordinated atoms with the central metal ions of the two cooper complexes.

Center	L_1^-	$[(CuL1)_2]$	L_2^-	$[(CuL2)_2]$
O_9	-0.64846	-0.66749	-0.64616	-0.75938
O_{18}	-0.80606	-0.68952	-0.80601	-0.69900
N_{11}	-0.36071	-0.31070	-0.31956	-0.35140
O_9	-0.64846	-0.67145	-0.64616	-0.66621
O_{18}	-0.80606	-0.69543	-0.80601	-0.66842
N_{11}	-0.36071	-0.31784	-0.31956	-0.23276

Table 7. Quantum global parameters, E_{HOMO} and E_{LUMO}, energy gap, Eg, ionization energy, I, electron affinity, A, electronegativity, χ, hardness, η, global softness, S, and chemical potential, V, of the ligands and copper complexes.

Parameter	L_1^-	$[(CuL1)_2]$	L_2^-	$[(CuL2)_2]$
E_T, au	-878.978	-2148.510	-993.331	-2377.101
E_{HOMO}, au	-0.05072	-0.18911	-0.06098	-0.19528
E_{LUMO}, au	0.05822	-0.15762	0.0598	-0.15846
E_g, eV	2.963	0.85652	0.285	1.0015
I, eV	1.3795	5.14379	1.6586	5.3116
A, eV	-1.5835	4.28726	-1.6265	4.31011
χ, eV	-0.102	4.71552	0.0160	4.8108
η, eV	1.4815	0.214135	1.6425	0.5007
S, eV	0.3374	2.33497	0.3044	0.9986
V, eV	-2.1712	-4.71552	-0.9718	-3.1565

Table 8. Non-quantum global parameters of the ligands ions and the complexes: Surface area grid (SAG), molar volume (MV), (log P), hydration energy (HE), polarizability (Pol), molar refractivity (MR) and mass (MW).

Parameter	L_1^-	$[(CuL1)_2]$	L_2^-	$[(CuL2)_2]$
SAG, Å^2	464.24	791.60	545.20	897.00
MV, Å^3	767.63	1466.95	902.32	1666.87
log P	2.80	4.33	1.91	2.56
HE, kcal mol^{-1}	-5.03	-14.21	-7.22	-14.31
Pol, Å^3	29.99	58.55	34.33	67.24
MR, Å^3	85.56	165.45	99.28	192.89
MW, amu	267.31	659.69	303.34	731.76

Table 9. Total static dipole moment (μ), the mean polarizability (α), the anisotropy of the polarizability ($\Delta\alpha$) and first order hyperpolarizability (β) of the ligands ions and the complexes.

Parameter	L_1^-	$[(CuL1)_2]$	L_2^-	$[(CuL2)_2]$
μ_x	-6.2423	-1.7742	-3.9297	-2.1248
μ_y	0.6129	1.3424	-4.4312	4.4153
μ_z	-1.5332	4.8748	-2.0088	-0.4450
μ, D	6.4569	5.3548	6.25406	4.92012
α_{xx}	-165.8107	-238.9810	-168.3159	-252.8339
α_{yy}	-157.5241	-231.7520	-170.4271	-254.6749
α_{zz}	-129.1993	-247.9899	-144.2745	-277.5419
α_{xy}	16.4126	0.4337	-4.9223	23.6007
α_{xz}	-4.3566	-1.7219	5.5405	-3.5847
α_{yz}	0.7243	1.7069	7.3209	-4.9427
α, au	-150.844	-239.574	-161.005	-261.685
α, esu	-2.235×10^{-23}	-3.550×10^{-23}	-2.386×10^{-23}	-3.878×10^{-23}
$\Delta\alpha$, au	33.2517	14.0905	25.1635	23.8031
β_{xxx}	-104.0948	-14.1243	-58.8850	34.2795
β_{yyy}	-59.7630	75.7340	-71.5709	120.9529
β_{zzz}	19.8294	-8.9697	-12.0768	47.5337
β_{xyy}	-17.0150	-0.4238	-25.5541	26.0251
β_{xxy}	67.7049	26.2451	34.3919	-11.3221
β_{xzz}	-7.5757	-17.9973	-19.1640	13.8704
β_{xxz}	-18.9820	-9.1014	37.0768	70.5336
β_{yzz}	7.2446	-0.2366	21.5118	-0.7065
β_{yyz}	-29.6504	30.4064	-22.3486	-30.6595
β_{xyz}	11.6346	32.2845	-0.8195	-24.1351
β, au	132.740	107.350	104.814	158.134
β, esu	1.146×10^{-30}	9.289×10^{-31}	9.055×10^{-31}	1.366×10^{-30}

Table 10. Thermogravimetric data orf the two copper complexes.

Complex	Decomposition step, °C	% Mass loss Found (Calc.)	M.Wt Found (Calc.)	Species eliminated	% Solid residue Found (calc.)
[(CuL1)$_2$]	120-371 374-799	38.44 (38.85) 42.08 (41.86)	253.56 (256.305) 276.78 (276.170)	$C_{15}H_{16}N_2O_2$ $C_{17}H_{12}N_2O_2$	127.25 (127.08) Copper metal
[(CuL2)$_2$]	125 -249 249-349 349-1000	12.60 (13.54) 40.73 (40.50) 37.63 (37.57)	92.20 (99.11) 298.05 (296.33) 273.15 (273.34)	$C_4H_7N_2O$ $C_{20}H_{12}N_2O$ $C_{14}H_9O_2$	127.31 (127.08) Copper metal

Table 11. Antimicrobial activities of the two copper complexes.

Sample	Diameter inhibition zone (mm)			
	E. coli (G^-)	*S. aureus* (G^+)	*A. flavus* (Fungus)	*C. albicans* (Fungus)
[(CuL1)$_2$]	21	20	10	10
[(CuL1)$_2$]	21	18	9	10
Ampicillin	25	21	--	--
Amphotericin B	--	--	17	19

Credit author statement

The contribution of every author is as follow:

Prof. Samir M. El-Medani: Shared in ideas, discussion and evolution of overarching the paper.

Prof. Abdelmoneim A. Makhlouf: Shared in design of experimental work and preparation of ligands.

Prof. Hussein Moustafa: Did the theoretical part (run and write the discussion).

Ms. Manal A. Afifi (a PhD candidate): Did the experimental part and shared in collecting literature and writing.

Dr. Matti Haukka: Did the crystal structure work.

Prof. Ramadan M. Ramadan: Shared in ideas, objective and aim of research as well as in writing discussion of the manuscript.

Declaration of interests

☒ The authors declare that they have no known competing financial interests or personal relationships that could have appeared to influence the work reported in this paper.

☐The authors declare the following financial interests/personal relationships which may be considered as potential competing interests:

Highlights

- Synthesis, characterization and spectroscopic studies of two phenylacetohydrazide Schiff base and their copper complexes.
- Spectroscopic studies and X-ray analysis of the Schiff base and its Cu complex as well as a dimer derivative.
- DFT calculations of the reported compounds.
- Biological studies including, antimicrobial and antioxidant activities of the complexes along with fluorescence quenching studies and viscosity measurements.
- Molecular docking of the two ligands and one copper complex.